applied sciences

MDPI

Review

Ice-Templated Porous Nanocellulose-Based Materials: Current Progress and Opportunities for Materials Engineering

Shubham Gupta [1,2], Florian Martoïa [2], Laurent Orgéas [1] and Pierre J. J. Dumont [2,*]

[1] University of Grenoble Alpes, CNRS, Grenoble INP, 3SR Lab, F-38000 Grenoble, France; shubham.gupta@3sr-grenoble.fr (S.G.); laurent.orgeas@3sr-grenoble.fr (L.O.)

[2] University of Lyon, INSA Lyon, CNRS UMR5259, LaMCoS, F-69621 Lyon, France; florian.martoia@insa-lyon.fr

* Correspondence: pierre.dumont@insa-lyon.fr; Tel.: +33-474-819-312

Received: 31 October 2018; Accepted: 21 November 2018; Published: 2 December 2018

Featured Application: Ice-templated nanocellulose-based materials are low-density biobased materials that constitute promising solutions for several engineering fields. They can be used in the building and car-manufacturing industry as heat/and or sound insulation board, as porous template for the storage and generation of energy, as membrane for fluid purification, or even as scaffold for biomedical applications.

Abstract: Nanocelluloses (cellulose nanocrystals, CNCs, or cellulose nanofibrils, CNFs) are the elementary reinforcing constituents of plant cell walls. Because of their pronounced slenderness and outstanding intrinsic mechanical properties, nanocelluloses constitute promising building blocks for the design of future biobased high-performance materials such as nanocomposites, dense and transparent films, continuous filaments, and aerogels and foams. The research interest in nanocellulose-based aerogels and foams is recent but growing rapidly. These materials have great potential in many engineering fields, including construction, transportation, energy, and biomedical sectors. Among the various processing routes used to obtain these materials, ice-templating is one of the most regarded, owing to its simplicity and versatility and the wide variety of porous materials that this technique can provide. The focus of this review is to discuss the current state of the art and understanding of ice-templated porous nanocellulose-based materials. We provide a review of the main forming processes that use the principle of ice-templating to produce porous nanocellulose-based materials and discuss the effect of processing conditions and suspension formulation on the resulting microstructures of the materials.

Keywords: nanocellulose; ice-templating; porous materials; process-induced microstructures

1. Introduction

Cellulose is one of the most abundant biopolymers on Earth [1–3]. This natural polymer is a long-chain polysaccharide, made up of 7000–20,000 β-(1→4)-linked anhydro-D-glucose units [4–6] that can be found in wood (hardwood and softwood), annual plants (hemp, flax, jute ramie), seeds (e.g., cotton coir, etc.), grasses (bamboo, bagasse, etc.), marine animals (tunicates), algae, fungi, invertebrates, and bacteria [7]. However, wood constitutes the main supply source for the production of cellulose-based materials owing to its wide availability worldwide [8,9]. In the following, we will mainly focus on the properties and uses of wood-based nanocelluloses (Figure 1)

In the hierarchical structure of plant cell walls, cellulose chains are aggregated in microfibrils that are few-nanometer-thick slender fibres (Figure 1a–c) [1–4,6,10,11]. The structure of microfibrils is also

semi-crystalline. However, the exact organisation of crystallites in the microfibrils is still not completely understood [5]. Recent studies [12,13] have shown that amorphous regions in microfibrils are very small and/or are presumably more correctly only "slightly disordered" and not fully amorphous. On a larger scale, the microfibrils themselves are aligned and bound in the form of bundles by hemicelluloses and either pectin or lignin (Figure 1c).

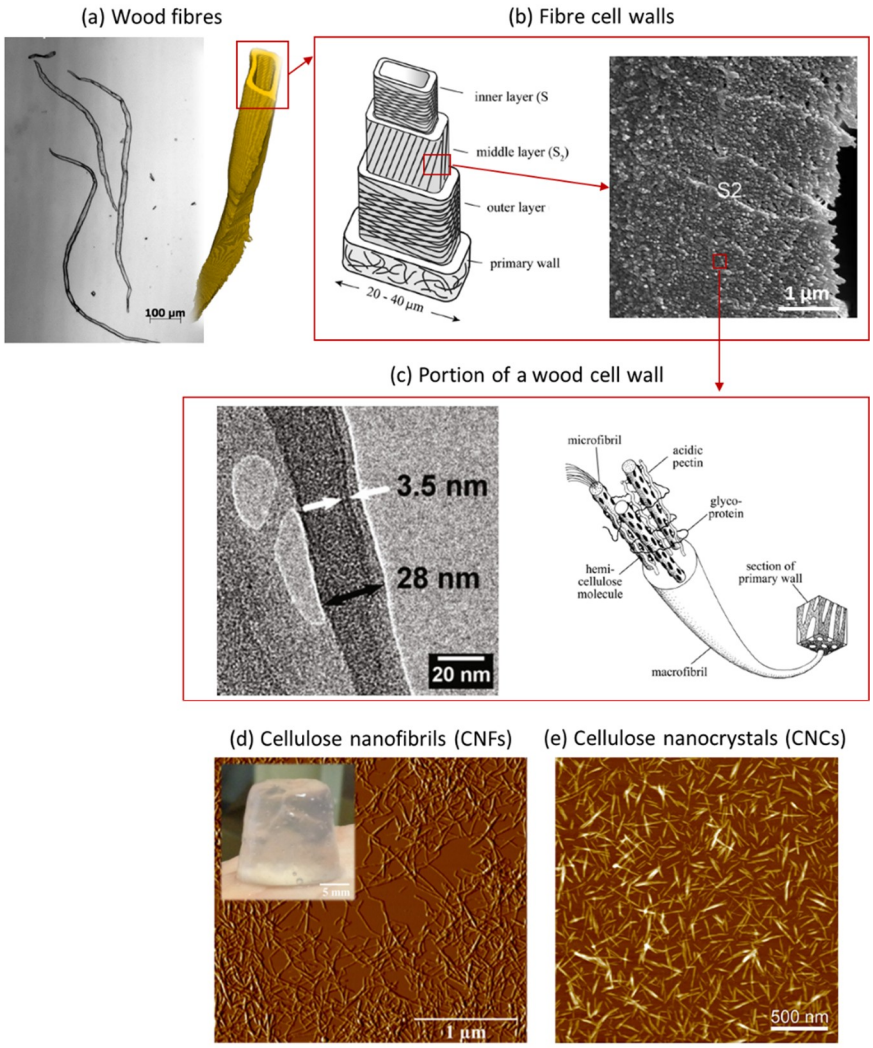

Figure 1. Hierarchical structure of wood fibres (**a**), showing the various layers (S1, S2, S3) in wood cell wall (**b**) [14] (Adapted from Donaldson [14] with permission from © Springer-Verlag 2007). (**c**) Portion of a wood cell wall showing the cellulose microfibrils aligned and bound in the form of bundles by hemicelluloses and lignin. (Adapted from Chinga-Carrasco [15] with permission from licensee Springer. 2011). Atomic Force Microscope (AFM) micrographs of CNFs (**d**) [16] and CNCs (**e**) (Adapted from Klemm et al. [5] with permission from Elsevier). In Figure (**d**), the photograph inset shows a TEMPO-oxidised CNF water suspension with solids content of 1 wt%. Note that the TEMPO-oxidation is a chemical pre-treatment used to improve the delamination of cellulose fibres. This pre-treatment leads to a regioselective oxidation of cellulose primary alcohol groups (–OH) at the surface of the fibrils into carboxylate ones ($–COO^-$). As such, negatively charged CNFs are more easily isolated from the fibre walls during the disintegration process [17,18].

Nanocelluloses (cellulose nanocrystals, CNCs, or cellulose nanofibrils, CNFs) are portions of plant cell walls with at least one dimension in the nanometer range [5,19,20]. CNFs (Figure 1d) are mechanically produced by delaminating plant-based cellulose, yielding slender nanoscale

fibrous particles (length l > 1 µm and width $d \approx$ 5–100 nm) containing both disordered and crystalline regions [1,5,20]. The delamination process of cellulose fibres is often combined with pre-treatments such as enzymatic hydrolysis [21,22], carboxylation via TEMPO-mediated oxidation or periodate chlorite oxidation [17,18], carboxymethylation [23], designed to reduce energy input needed for fibrillation. As such, CNFs present a wide diversity of microstructures and surface chemistries. In contrast, CNCs (Figure 1e) are mainly extracted from cellulose fibres using an acid hydrolysis process [20,24]. The isolation of CNCs by acid hydrolysis selectively degrades disordered cellulose chains, resulting in highly crystalline rod-shaped nanoparticles [5]. CNCs are considerably less slender than CNFs (length $l \approx$ 100–200 nm and width $d \approx$ 5–20 nm). Many review articles [6,8,25–27] and books [20,28] dealing with the production processes of nanocelluloses are available for interested readers.

Nanocelluloses in the form of CNCs and CNFs have received considerable attention over the last two decades. CNCs and CNFs combine important cellulose properties (e.g, a low density, high mechanical properties, the possibility to modify the surface chemistry) with the features of nanomaterials (e.g., high aspect ratio l/d, few internal defects, high specific surface area, etc.) [1,3,5,29,30]. These cellulosic nanoparticles are used as building blocks for novel biobased engineering materials [29] such as nanocomposites [1,31,32], densely packed and transparent nanocellulose films [33,34], continuous filaments [35,36], and aerogels [37–39] and foams [40–42]. The research interest in nanocellulose-based aerogels and foams is recent but growing rapidly. Porous materials in the form of foams and aerogels exhibit unique properties such as a low density, high specific surface area, excellent deformability, the ability to absorb the shocks and/or to have good sound and thermal insulation properties [43–45]. These materials are increasingly used in an ever-wider variety of engineering fields. However, foams and aerogels are usually synthesised from polymer or carbon-based materials, most of which are derived from petroleum-based products. The reasons for the growing interest in nanocellulose-based foams and aerogels are explained by the desire to move toward renewable raw materials and more sustainable resources and processes. Nanocellulose-based foams and aerogels display high porosity [37,46], interesting mechanical behavior characterised by a great deformability under compression [47–49], high thermal insulation properties [37,41], and potential bio-compatibility [46,50,51], which make them promising solutions for several engineering fields [52]. These materials can be used in the building and car-manufacturing industry as heat/and or sound insulation board, as porous template for storage and generation of energy, as membrane for fluid purification, or even as scaffold for biomedical applications.

The forming processes of aerogels and foams commonly involve two main steps, namely (i) the preparation of nanocellulose suspensions/gels or wet foams, and (ii) removal of the suspending fluid. As shown in Figure 2, the removal of the suspending fluid can be carried out using various drying procedures such as convective drying [53,54], supercritical drying [37,39,55] and solidification combined with freeze-drying, also referred to as "ice-templating" [40,56]. Depending on the chosen processing route, various porous structures can be obtained: (i) aerogels of ultra-high porosity (>90%) and with nanosized pores (average pore size $d \approx$ 2–50 nm), and (ii) cellular materials in the form of foams of medium to high porosity (>50%) and with microsized pores ($d \approx$ 10–500 µm) [52].

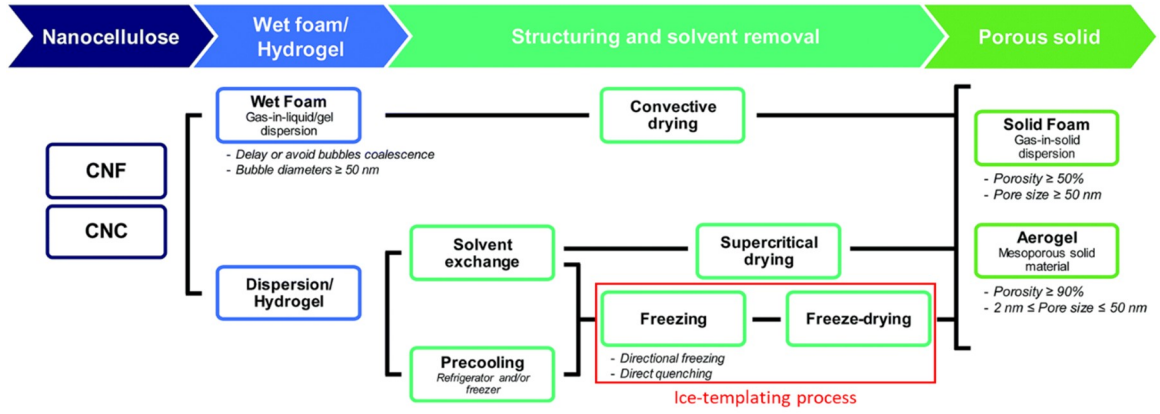

Figure 2. Schematic view of the different processing routes used to obtain nanocellulose-based aerogels and foams. (Adapted from Lavoine and Bergström [52] with permission from the Royal Society of Chemistry); CNF: cellulose nanofibril, CNC: cellulose nanocrystal.

This review focuses on the fabrication of porous nanocellulose-based materials obtained by ice templating, i.e., after freezing of suspensions and sublimation of the formed ice crystals (freeze-drying). The materials obtained with this approach commonly exhibit a foam-like structure with open porosity and micrometric cells. This technique is interesting owing to its simplicity and versatility, and constitutes an eco-friendly alternative (most of the time the solvent used is water) for the design of biobased lightweight materials. Hence, the main objective of this review is to describe and discuss the various materials, microstructures, and end-use properties that can be obtained, changing or tuning the forming conditions and/or the characteristics of nanocellulose suspensions/gels.

2. Basis of Ice-Templating

The use of freezing colloids as a route to template porosity in materials, usually called ice-templating, although known for many years [57–59], has been the subject of considerable attention over the last ten years [60–63]. The reasons for the growing interest in utilising ice-templating process in materials engineering stem from its simplicity and versatility and the wide variety of porous materials that this technique can provide. The basic principle of ice-templating is simple: it is a segregation-induced templating of a dispersed (or dissolved) solid phase by a solidifying solvent (Figure 3). The dispersed (or dissolved) phase can be of almost any nature, from ceramic to metal particles or polymer. During the solidification of the suspension, the dispersed (or dissolved) phase is rejected from the growing crystals of the solvent. The solidified solvent is then removed by sublimation, leaving a template porous material where the pores are almost a direct replica of the frozen solvent crystals.

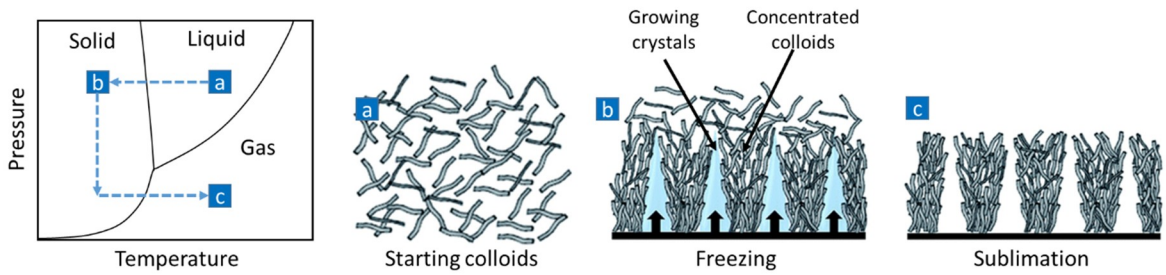

Figure 3. Scheme of the principle of ice-templating. (Adapted from Lavoine and Bergström [52] with permission from the Royal Society of Chemistry).

In practice, the processing of porous materials by ice-templating can be divided in three main steps (Figure 3).

a. Preparation of the suspensions. The solid phase is dispersed (or dissolved) in the liquid medium (solvent). The stability of the suspension should be carefully controlled to avoid any segregation phenomenon taking place in the solidification phase, yielding gradients of porosity in the final materials. Water is the most commonly used solvent because it is easy to use and manipulate and available in large quantities [63]. Other solvents such as camphene [64,65] and ter-butyl alcohol (TBA) [66,67] are also frequently used in the ice-templating process. Generally, moderate solid loading is used (10–40 vol.%) to ensure that crystals have enough space to grow and solid particles are redistributed by the crystals. The concentration of solids in the initial suspension should be adjusted to reach the desired porosity in the final materials.

b. Solidification of the suspensions. During this step, crystals of solvent are formed and grow in the suspension. The solid particles that are dispersed (or solubilised) in the suspension are rejected by the moving solidification front, concentrated, and entrapped between the crystals. This step is crucial and determines the characteristics of the porous structure (e.g., shape, size of the pores) in the final materials. The freezing conditions mainly depend on the choice of the solvent [63]: for instance, low temperatures (<0 °C) are required when using water, whereas room temperature is sufficient when using camphene. It is important to notice that the equipment required to fabricate the materials (e.g., the mould) has to accommodate the variations of volume (e.g., −3.1% for camphene, 9% for water [63]) that can occur during the solidification of the suspensions.

c. Sublimation of the solvent. After complete solidification of the suspension, the sample is kept at conditions of low temperature and reduced pressure using a freeze-drying equipment [68]. The sublimation conditions are dictated by the physical properties of the solvent. Under these conditions, the solidified solvent is converted into a gas, leading to a porous structure.

The ice-templating process has already been used to fabricate a wide variety of porous materials with a great potential in several engineering fields [63], including construction [69], energy [70], and biomedical [71,72] sectors. In comparison to other processes, ice-templating routes exhibit several unique features. First, this process is almost material agnostic, i.e., almost any type of materials can be used. Ceramics [73], glasses [74], metals [75], carbon [76], and polymers [77] have already been used to design materials with various functional properties, including electrical, dielectric, catalytic, piezoelectric, acoustic, thermal, and mechanical properties. Secondly, a variety of porous structures (anisotropy, size, polydispersity of the pores) can be obtained depending on the choice of the solvent suspension formulation (solid content, additives), and the solidification conditions (temperature gradient, cooling rate, and so on). Thirdly, beyond the porous structures of the processed materials, a variety of shapes or "architectures" (thin filaments [78], structural foams [79], films and membranes [80], extruded metamaterials [81], microspheres [82]) can be obtained, depending on the chosen forming process. Many review articles [61,62,83] and books [63,84] give insights into the main achievements obtained up to date with this technique. However, very few studies [52,85] provide a complete review of the results, potentialities, and limitations obtained with nanocellulose-based systems. Thus, this review focuses on ice-templated materials processed from nanocellulose. It is organised as follows. In Section 3, we give a summary of the various types of nanocellulose suspensions and the shaping and forming processes (using the principle of ice-templating) that are commonly used to obtain porous nanocellulose-based materials. We also provide insights into the main applications of the processed materials. Then, in Section 4, we describe in detail how the microstructure of ice-templated materials can be tuned, depending on the choice of the nanocellulose suspensions, their formulation, and the processing conditions.

3. Ice-Templating of Nanocellulose Suspensions

The processing of nanocellulose-based materials by ice-templating involves (i) the formulation of nanocellulose suspensions and (ii) the use of forming processes that enable the suspensions to be solidified and sublimated under controlled conditions. This part aims at describing how nanocellulose

suspensions are commonly prepared and at giving a review of the main forming processes used to produce ice-templated porous nanocellulose-based materials.

3.1. Preparation of Nanocellulose Gels

As mentioned in the introduction, CNCs and CNFs are extracted from cellulose fibres by mechanical and/or chemical processing routes in the form of aqueous colloidal suspensions. Because of its hydrogen bonding ability and polarity, water is a good dispersant for the CNCs and CNFs that exhibit many hydroxyl groups (–OH) at their surface. CNF suspensions are commonly manufactured at a nanofibre concentration of about 1–2 wt% [8,20,26]. Due to the high aspect ratio of CNFs ($100 < l/d < 500$), their suspensions tend to form highly viscous gels even at very low nanofibre content. In contrast, the less slender CNCs ($l/d < 100$) can be produced at higher concentrations, typically from 5 to 15 wt% [34]. Depending on the extraction processes, the homogeneity and colloidal stability of nanocellulose suspensions are different [16,26]:

- CNF suspensions produced by mechanical disintegration with or without enzymatic pre-treatment [16,86,87] commonly exhibit heterogeneous mesostructures, characterised by the presence of mesoscale flocs or aggregates. At a finer scale, these suspensions contain both microscale elements such as partially fibrillated cellulose fibres but also nanoscale elements in the form of elementary fibrils or bundles of fibrils with a diameter that ranges between 5 and 100 nm and a length that ranges between 1 and 10 μm [16,88].
- In contrast, CNFs suspensions prepared using chemical pre-treatments of cellulose fibres such as carboxymethylation [23], carboxylation [17,18], and quaternisation [89] prior to mechanical treatment are less polydisperse suspensions that contain a few fibril bundles and mostly individualised fibrils having a diameter ranging from 3 to 6 nm and a length from 1 to 2 μm. The aforementioned chemical pre-treatments consist of a chemical modification of hydroxyl groups (–OH) at the surface of the fibrils to functional polar groups [26]. Therefore, at low ionic strength, i.e., without the addition of salts and/or additives, CNF aqueous suspensions are homogeneous, nearly transparent (Figure 1d), and electrostatically stabilised by the presence of negatively (or positively) charged groups at their surface [90,91].
- Similarly, CNC suspensions that are mainly produced from the hydrolysis by sulphuric acid of cellulose fibres, are homogeneous and electrostatically stabilised colloidal systems [92].

Using specific and time-consuming drying techniques [93,94], CNC and CNF suspensions can be concentrated up to 20 and 10 wt%, respectively [95,96]. However, the most concentrated suspensions are usually extremely viscous and thus are difficult to use in forming processes. Nanocellulose suspensions are colloidal fibrous systems that exhibit complex rheology between that of soft solids and liquids [16]. The rheology of these systems is usually characterised using transient and steady-state shear experiments (Figure 4) [97,98].

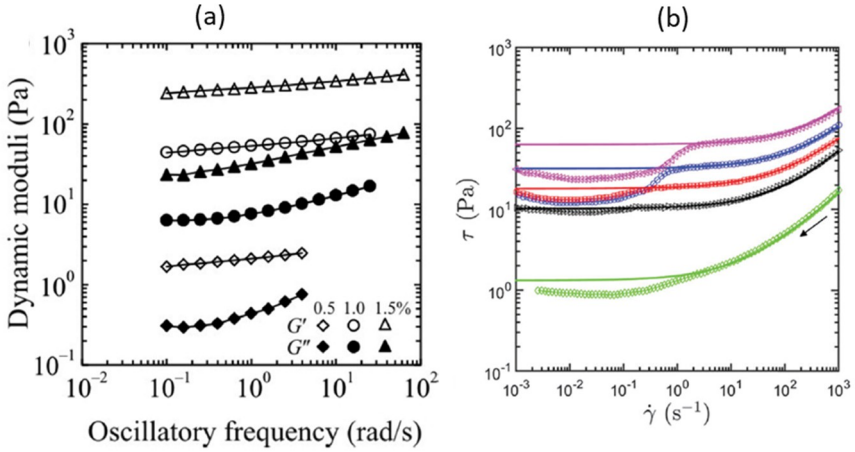

Figure 4. (**a**) Storage G′ and loss G″ moduli as a function of the oscillatory frequency for TEMPO-oxidised CNF suspensions at different concentrations (0.5–1.5 wt%). (Adapted from Nechyporchuk et al. [99]. Copyright 2015 Springer Science + Business Media Dordrecht. With permission of Springer). (**b**) Macroscopic flow curves (shear stress τ as a function of the shear rate $\dot{\gamma}$) obtained for various TEMPO-oxidised CNF suspensions concentrated at 0.3, 0.56, 0.7, 0.85, and 1 wt% using a plate–plate rheometer. In graph (**b**), the solid lines represent the fits of the Herschel–Bulkley model $\tau = \tau_0 + k\dot{\gamma}^n$, where k and n are the consistency parameter and the flow index, respectively. (Adapted from Martoïa et al. [100] with permission from the Royal Society of Chemistry).

At low strains and/or low strain-rates, the rheology of these systems is characterised by a solid-like behaviour [16]. The dynamic oscillation curves (e.g., Figure 4a) that are performed at small prestrains for CNC and CNF suspensions, show typical features of gels and soft glassy materials [101–103] with a storage modulus G′ much higher than the loss modulus G″. The solid-like properties of nanocellulose suspensions can also be observed from steady-state flow curves (e.g., Figure 4b). As shown in Figure 4b, CNF suspensions exhibit a macroscale yield stress τ_0 at low strain-rates [100,104–106]. This regime is then followed by a shear-thinning behaviour, where the suspension viscosity decreases with increasing the strain-rates [107]. The rheological properties of the suspensions, namely the dynamic modulus G′, the yield stress τ_0 and the viscosity μ of the suspensions are power-law functions of the nanofibre concentration [104,105,108]. These macroscale rheological properties, which are of great importance in materials forming, are closely related to the current microstructure of the fibrous reinforcement and its evolution during flow, and to a combination of nanoscale fluid-particles and particles-particles interaction forces [35,100,109]. More information related to the rheology of nanocellulose suspensions can be found in recent review articles [97,98].

Water is commonly used as suspending fluid, but stable suspensions of CNCs and CNFs can also be obtained in various polar liquid media. For example, stable CNC suspensions have been prepared in dimethyl sulfoxide (DMSO), *N*-methyl pyrrolidine (NMP), formic acid, and *N*,*N*-dimethyl sulfoxide (DMF) [110]. CNCs and CNFs can also be dispersed in other liquid media using solvent exchange procedures. The aqueous suspensions are progressively solvent exchanged in liquids of decreasing polarity by several successive centrifugation and redispersion operations, using sonication treatment after each solvent exchange step to avoid aggregation of the particles. Acetone is often chosen as solvent for the first solvent exchange step. To increase the stability of CNCs and CNFs in apolar or low polarity solvent, the surface of cellulose nanoparticles can be coated with surfactants [111], or chemically modified using various chemical grafting processes [112]. Both methods allow the surface energy of the nanoparticles to be decreased. More details related to the surface modification of nanocelluloses can be found in the following references [113,114].

3.2. Forming Processes

In the sections that follow, we provide a review of the main forming techniques used to produce porous nanocellulose-based materials with varied shapes and microstructures.

3.2.1. Freeze-Casting/Freeze Moulding Processes

This forming process involves the preparation of a colloidal suspension that is poured into a mould, which is then frozen and subjected to sublimative drying of the suspending fluid under vacuum. This approach has first been developed as a near-net-shape manufacturing process to obtain complex-shaped (monolithic) dense ceramics parts with fine replicate of the mould details [59,115]. However, in that case the formation and growth of ice crystals was unwelcome, as they turn into defects in the final materials. Later, it was realised that the crystal nucleation and growth could be a benefit if properly controlled to obtain materials with porous microstructures [116].

Various strategies can be used to achieve complete freezing of the nanocellulose suspensions. A first strategy consists in progressively introducing the mould filled with the suspension in a cold liquid (Figure 5a) [40,117–119]. Changing the temperature of the liquid bath enables the cooling rate of nanocellulose suspensions to be varied [56,118]. Also, the establishment of the temperature gradient within the moulds can be tuned by using moulds with different thermal resistances. For instance, Jiménez-Saelices et al. [119] designed a mould composed of three parts: the top and bottom surfaces were made of high thermal conductivity aluminium, whereas the lateral edges were made of low thermal conductivity polymer. This mould design allowed a quasi-unidirectional temperature gradient to be applied to the nanocellulose suspensions. A second strategy is to deposit the mould on a cold surface, leading to the unidirectional freezing of the suspensions [41,120,121]. In addition, the freezing of the suspension can also be achieved by placing the mould inside a cold chamber [122–124]. However, this last way of freezing does not allow a good control of the temperature gradient inside the mould. After complete freezing of the suspensions, the dehydration process is commonly carried out by placing the frozen samples inside freeze-dryer apparatus.

This forming process enables thick foam panels with densities ρ ranging from 1 to 200 kg m^{-3} (i.e., a porosity ranging from 99% to 87%) to be produced (Figure 5). The density (or the porosity) of the final materials depends on the initial concentration C_i of the nanocellulose suspension and volumetric shrinkage that is prone to occur during the sublimation of ice-crystals. Martoïa et al. [56] observed that the foam shrinkage increased drastically when C_i was lower than a critical concentration C*. This critical concentration C* was found to depend on the nanofibre slenderness and colloidal interactions between the particles.

At a finer scale, the foams produced using this process commonly exhibit a cellular-like architecture (Figure 5c,d). The morphology of the cells is different from that usually observed in most of the synthetic polymer cellular foams. Instead of the polyhedral cells typical of many foams [43], nanocellulose foams consist of irregular arrangements of thin plates (in the form of nanocellulose films [40,125]), tens of microns in length that occasionally intersected with remaining partially fibres or dangling mass [56]. The plates themselves are curved and nanoporous [40,56]. However, the pore structure of these materials is almost a direct replica of the ice-crystals formed during the freezing process, and therefore this structure ultimately depends on the freezing conditions (e.g., temperature gradient and cooling rate) [62]. This point will be discussed further in Section 4.

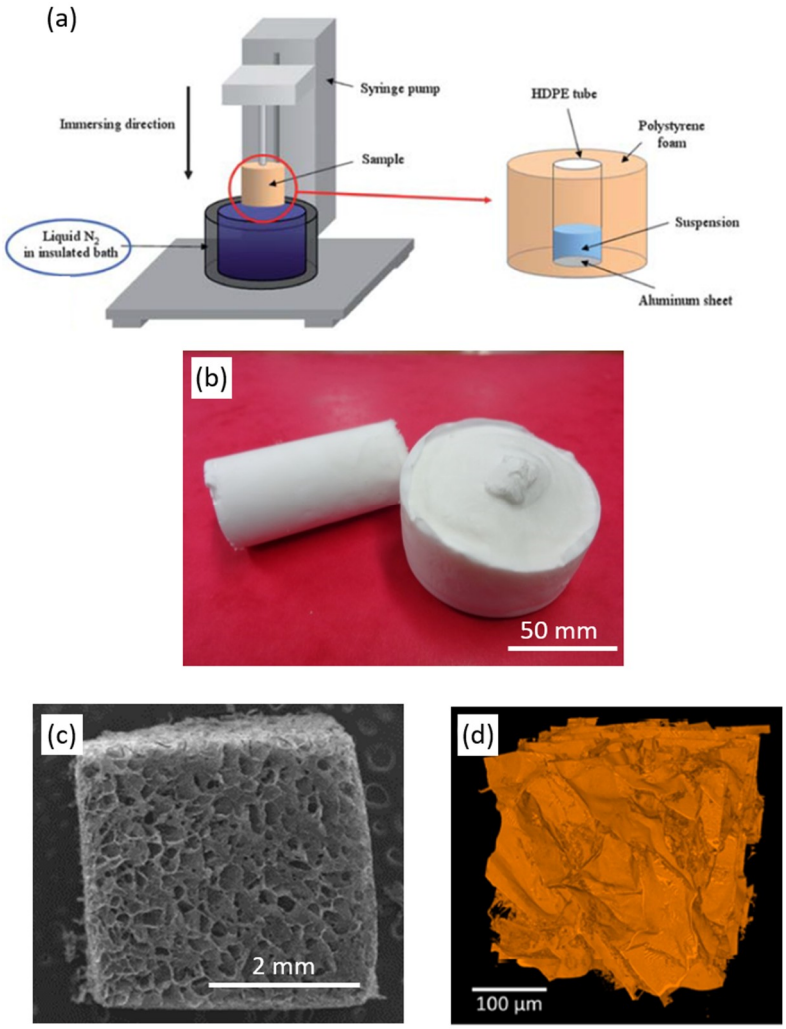

Figure 5. (**a**) Scheme of a freezing apparatus. The nanocellulose suspension is frozen by introducing the mould in a cold liquid. (Adapted from Lee et al. [118] with permission from the Royal Society of Chemistry). Photograph (**b**), Scanning Electron Microscopy (SEM) micrograph (**c**), and 3D tomographic image (voxel size: 0.32^3 µm^3) (**d**) of TEMPO-oxidised CNF foam ($\rho \approx 11$ kg m^{-3}) prepared by direct quenching in a cold bath (freezing temperature T ≈ -13 °C). (Adapted from Martoïa et al. [56] with permission from Elsevier).

3.2.2. "Sorbet-Like" Processes

Martoïa et al. [56] used an alternate freezing processing route inspired from the food industry or the metallurgy to process metals for thixocasting [126,127]. The authors combined several sequences of quenching and mechanical stirring to obtain nanocellulose foams. The purpose of this technique was to restrain the dendritic and columnar ice crystal growth during solidification of the suspensions by applying mechanical stirring to obtain a first class of ice grains with globular shape. In practice, nanocellulose suspensions were continuously mixed at a temperature of T ≈ -18 °C until the suspensions exhibited ice-cream textures. Then, the mould was filled with the suspensions before being quenched at low temperature (T ≈ -68 °C) to completely solidify the suspensions. At the end of the solidification process, frozen suspensions were dried in a freeze-dryer.

The materials obtained using this forming process exhibited interesting bimodal structures that consisted of near spherical mesoscale pores/cells with a diameter that ranged from 100 µm to 600 µm (Figure 6). These cells were flanked by finer anisotropic pores/cells in the form of buttresses with dimensions that ranged between 20 and 50 µm. Interestingly, the authors observed that the foams

prepared using this "sorbet-like process" showed higher mechanical performances than foams with the same density and prepared by freeze-moulding. These porous materials can be used in the design of lightweight composite structures (e.g., as a core of sandwich panels), for which high specific mechanical properties are needed.

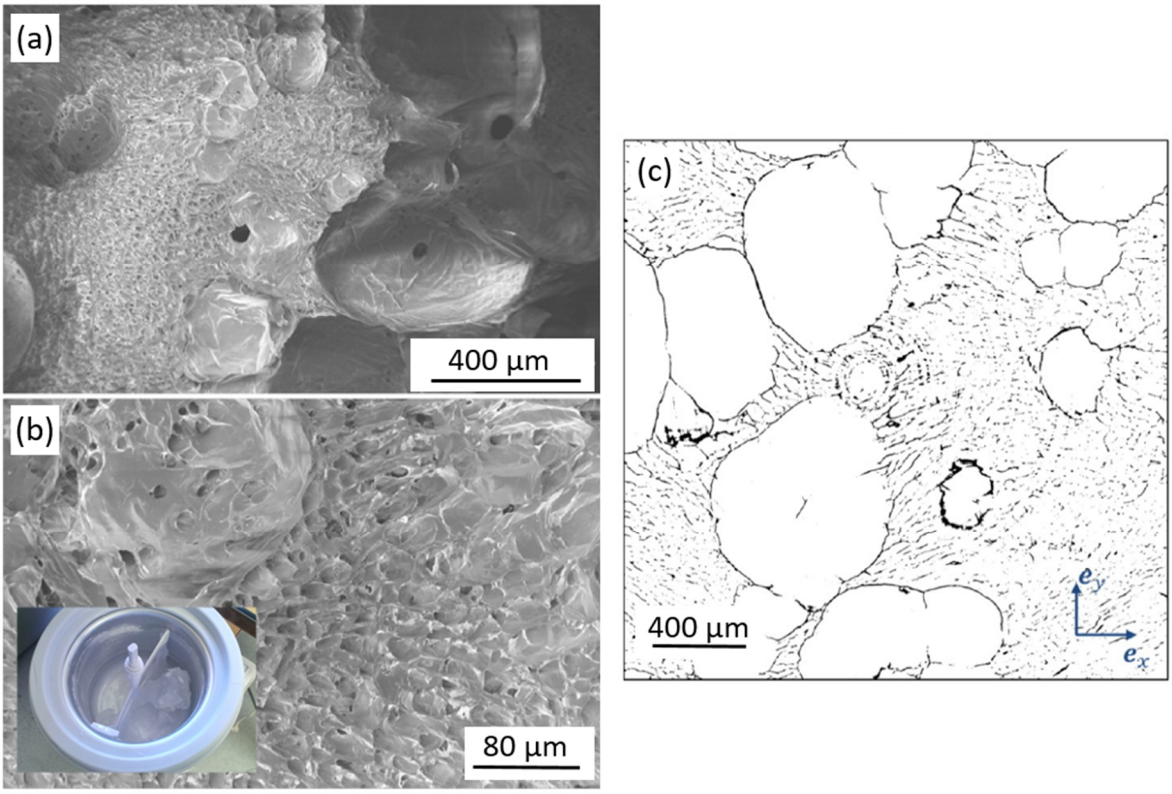

Figure 6. (**a**) SEM micrographs showing the microstructures of a TEMPO-oxidised CNF foam obtained using a sorbet-like process. In (**b**), the photograph inset shows the sorbet machine used to apply mechanical stirring during the freezing of CNF suspensions. (**c**) Horizontal cross-section of the TEMPO-oxidised foam obtained using X-ray microtomography (voxel size: 1.6^3 µm^3). (Adapted from Martoïa et al. [56] with permission from Elsevier).

3.2.3. Spray-Freeze Drying Processes

The atomisation and spray-freeze-drying (SFD) process was used by Cai et al. [128] for the fabrication of porous nanocellulose-based microspheres. Spray-freeze drying is a process that was originally developed for the production of biopharmaceutical powder [129]. In SFD, a suspension of CNFs or CNCs is sprayed with an air-atomisation nozzle into a cold vapour phase over a cryogenic liquid to form droplets (Figure 7). The droplets of the suspension may begin to freeze during the time of flight through the cold vapour phase and completely solidify upon contact with the cryogenic liquid phase. Then, the frozen droplets are dried in a lyophiliser.

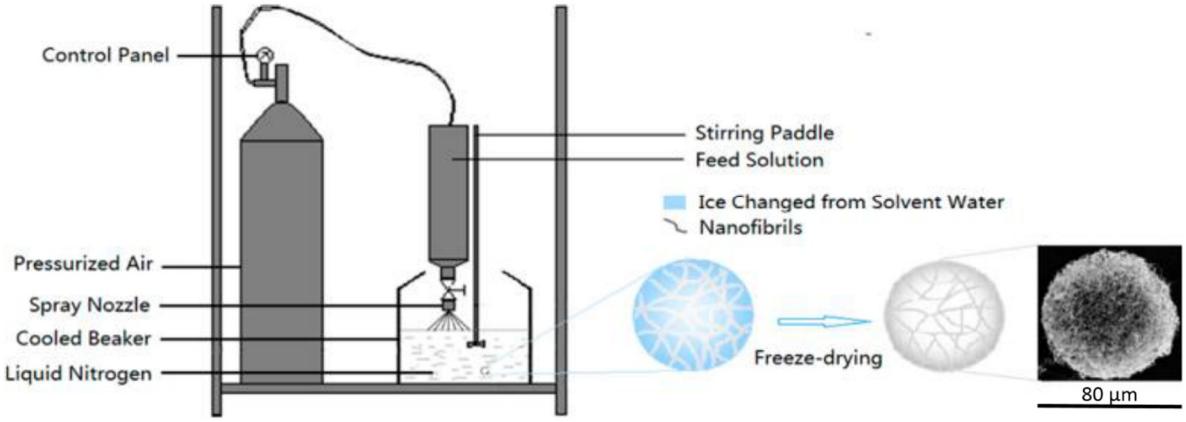

Figure 7. Scheme of the atomisation and spray-freeze-drying process used for the fabrication of porous microspheres. (Adapted with permission from Cai et al. [128]. Copyright 2014 American Chemical Society).

Using this approach, the authors produced porous nanocellulose-based microspheres (Figure 7) with an average diameter of about 60–120 µm [128]. In addition, the microbeads had a porous structure with pore sizes ranging from a few nanometers to micrometers. Microspheres are promising materials that can be used a template for drug delivery, superabsorbents, synthesising porous catalysts, cell culture growth templates, and targeted release systems.

3.2.4. Extrusion Processes

This process consists of printing 3D structures with controlled shapes from nanocellulose gels (Figure 8). To be printable in a 3D printer, the fluid needs to flow in the printer and have the ability to become like a "solid" on a substrate after being dispensed (Figure 8b) [130]. As mentioned in Section 3.1, nanocellulose suspensions are yield stress fluids that are characterised by a pronounced shear thinning behaviour at high strain-rates [100,107]. Hence, these suspensions are particularly suitable for this type of processing route. The mechanical stresses applied on the nanocellulose gels inside the nozzle in the printer head decreases the viscosity of the gel and the fluid starts to flow. However, as the nanocellulose gel is deposited, the stresses reduce so that the fluid relaxes and forms a solid-like gel, making it possible to build a 3D structure (Figure 8b).

Then, in order to create a stronger structure that is easier to move and handle without breaking, the 3D printed structure can be transferred to a coagulation bath (e.g., $CaCl_2$ bath [131]). This reduces the repulsive surface charges of the cellulose nanoparticles, so that they can be physically cross-linked through attractive cohesive bonds [35,90]. Then, the 3D printed structure is frozen and freeze-dried (Figure 8c). Using this approach, it is possible to achieve materials with porosity defined at several scales (Figure 8d): the pores defined by the extrusion (computer designed) and the ice-templated pores [132]. These materials have great potential in tissue engineering applications as culture scaffolds due to their multiscale open-cell type porous structures. Hence, cell growth can migrate through the designed cellulosic-scaffold using the smaller to medium pore sizes. Meanwhile, the larger pore sizes can enable nutrient and metabolic waste diffusion to occur simultaneously until complete cell migration is achieved. This demonstrates how ice-templating can be combined with other processing routes to achieve complex and customisable architectures suited for target application requirements.

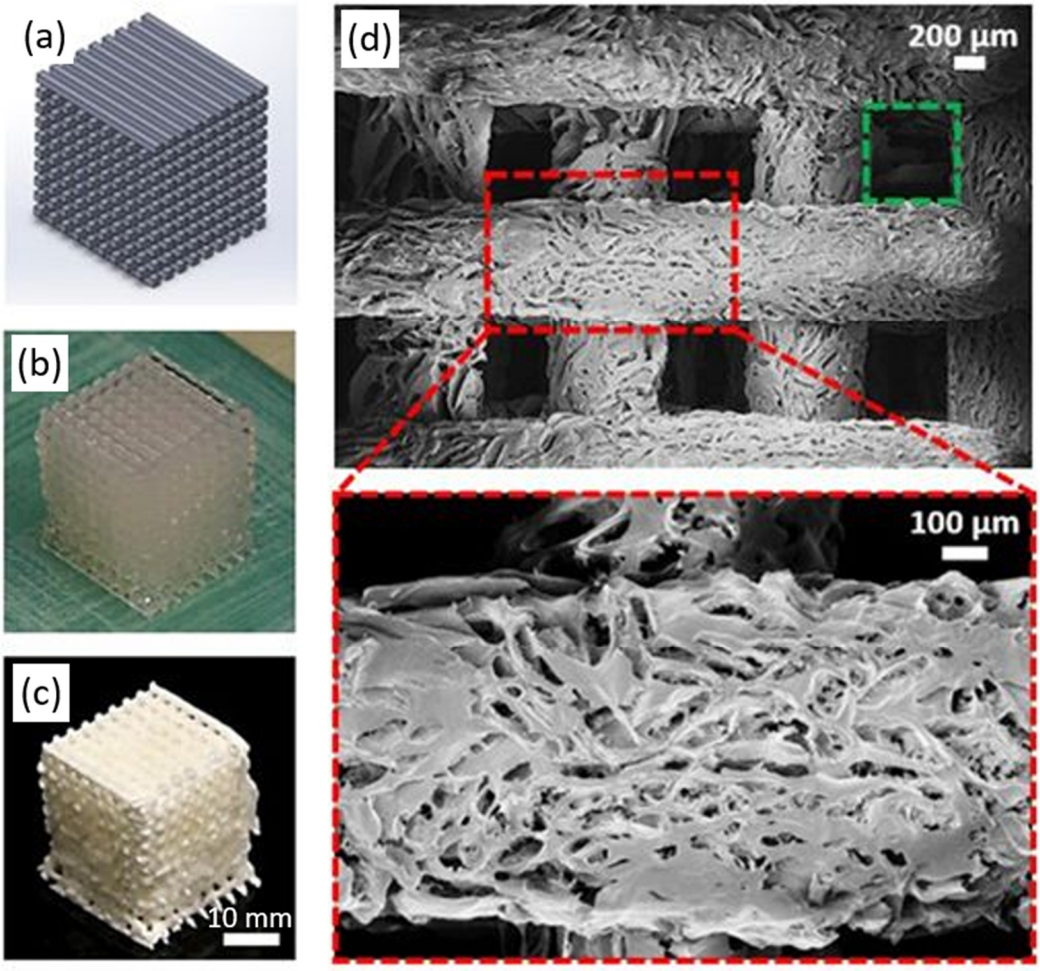

Figure 8. 3D printed scaffold obtained using a direct ink write (DIW) approach: (**a**) CAD model, (**b**) 3D structure obtained after direct printing of a 20 wt% CNC gel and (**c**) final structure obtained after freezing in a freezer at a temperature of −20 °C and sublimation. (**d**) SEM images showing the dual scale porosity of the fabricated materials: large pores of about 600-µm diameter (green box) defined by the extrusion process coexist with finer elongated pores (red box) induced by the ice-templating process. (Reproduced with permission from Li et al. [132]).

3.2.5. Post-Treatment Processes

Interestingly, ice-templated nanocellulose-based materials can also be used as "template" for the design of novel engineered materials. For instance, Nissilä et al. [133] used CNF foams as anisotropic porous preform for the fabrication of nanocomposite materials. Anisotropic porous CNF foams were impregnated with an epoxy resin using a vacuum infusion process (Figure 9a). This composite forming process uses a low vacuum pressure ($\Delta P \approx 35$ mbar) to slowly push the uncured resin of low viscosity into the porous medium. Once the resin is entirely infused, a chemical reaction creates heat, curing the resin into a solid part. This technique allows the fabrication of eco-friendly structural composite parts that could have a great potential in many engineering fields. Wang et al. [134] produced carbon-based ultralight materials by pyrolysing TEMPO-oxidised foams at 1000 °C under nitrogen flow. After pyrolysis, as shown in Figure 9b, the volume of carbon foams shrank by about 75% compared with the original volume of CNF foams. Also, the weight loss reached 75% due to the release of water, CO_2, CO, CH_4, and some organics [135]. However, the porosity of the pyrolysed sample was still very high (porosity ≈ 99.5%) and a finer analysis of the microstructure revealed that the 3D porous structures of the foams was well maintained [134]. The unique properties of carbon foams such as their high porosity and specific surface area, combined with the advantages of using a natural and

sustainable material, make them promising materials for energy storage applications as electrode materials and super-capacitors.

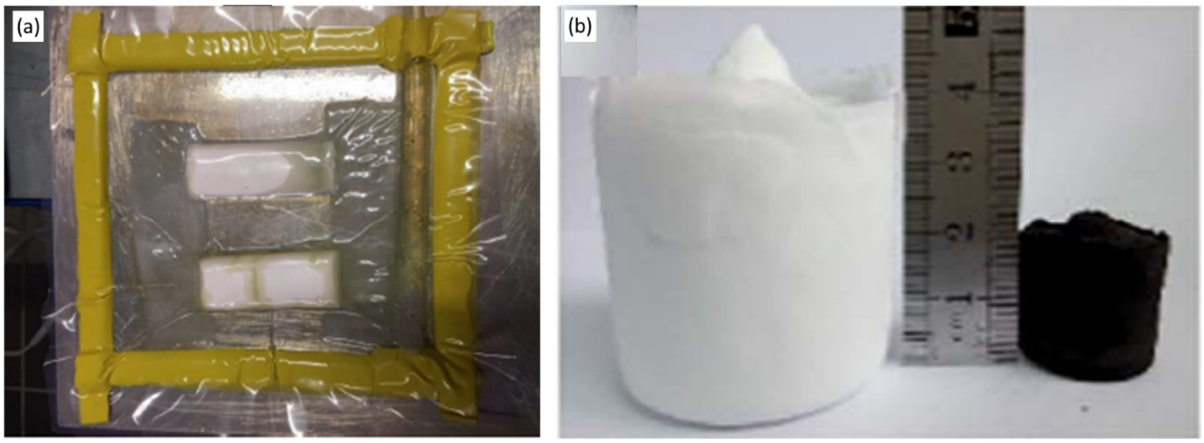

Figure 9. Examples of post-treatment processes of ice-templated porous nanocellulose-based materials. (**a**) Vacuum infusion of a CNF foam with an epoxy resin to obtain a composite material (Adapted from Nissilä et al. [133] with permission from Elsevier). (**b**) Photograph of a carbon foam (black sample on the right) obtained from the pyrolysis of a CNF foam (sample on the left) under nitrogen flow. (Adapted from Wang et al. [134] with permission from the Royal Society of Chemistry).

4. Links between the Nanocellulose Suspensions, the Processing Conditions, and the Microstructures of Ice-Templated Materials

The control of the arrangement and organisation of solid particles during the solvent solidification phase is complex and still not fully characterised and understood [62,63]. The mechanisms of particle segregation and redistribution induced by ice-crystal growth in colloidal systems depend on a large number of factors related both to the processing conditions and the nature of colloids (particles, size, surface charge density, conductivity, etc.). Hence, this section aims at describing how ice-templating conditions and suspension formulation affect the final microstructures of nanocellulose-based materials.

4.1. Effect of Freezing Conditions

4.1.1. Temperature Gradient

Temperature gradient has a drastic effect on the process-induced microstructures and the morphology of the pores/cells [119]. Anisotropic pores (the long pore axis being parallel to the freezing direction) were observed for CNF and CNC foams produced using a unidirectional freezing process [41,118,120,136,137]. Ice crystals tend to grow in the same direction as the temperature gradient. Consequently, the directional solidification of nanocellulose suspensions leads to a crystal alignment that leaves open pore channels after sublimation (Figure 10).

The effect of the temperature gradient on the final microstructures of ice-templated nanocellulose-based materials was investigated in refs. [117,119]. In Ref. [119], the authors used two different moulds to apply different freezing gradients to the nanocellulose suspensions. The first mould was designed to induce a quasi-uniaxial temperature gradient in CNF suspension, whereas the second was designed to apply a quasi-uniform temperature gradient. The first mould lead to ice-templated foams with highly anisotropic and columnar structures and the second mould to more isotropic cellular microstructures with more spherical pores.

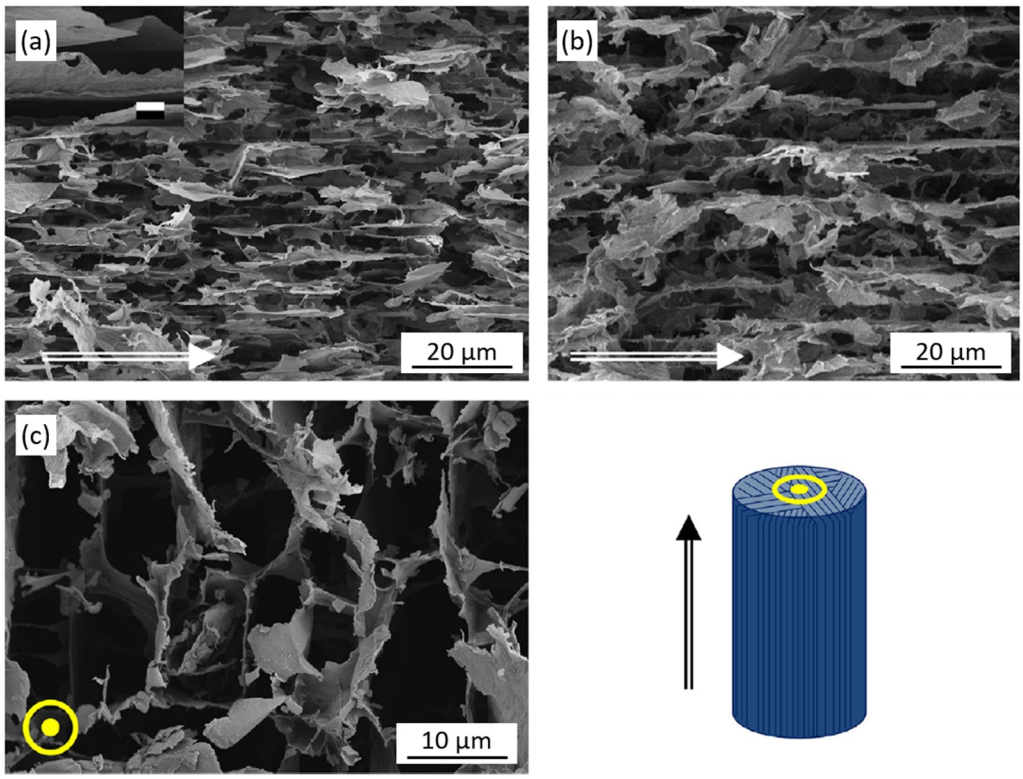

Figure 10. SEM micrographs showing the microstructures of CNF foams that were obtained after unidirectional freezing and sublimation. In figure (**a**,**b**), the CNF foam was cut parallel to the freezing direction (indicated by arrow), whereas in figure (**c**) the foam was cut perpendicular to the freezing direction. (Adapted from Donius et al. [136] with permission from Elsevier).

4.1.2. Cooling Rate

Martoïa et al. [56] showed that the morphology of the pores/cells also varied significantly as a function of the freezing temperature. Between −13 °C and −80 °C, the radial pore size decreased from few hundred microns (300–50 µm) to a few tenths of micrometers (20–10 µm) for TEMPO-oxidised and enzymatic CNF foams (Figure 11). In addition, CNF foams obtained at high freezing temperature, i.e., T = −13 °C consisted of cells that were more polydisperse compared with those observed in foams that were obtained at lower freezing temperatures. Also, between −80 °C and −114 °C, no significant variation in the pore morphology and size was evidenced (Figure 11). These variations in the pore morphology, which were observed for CNCs and CNFs and for various concentrations, could be explained by the following scenario. At low freezing temperature and thus high average cooling rate, nucleation rate is higher than crystal growth rate [138]. Consequently, a large number of small ice crystals are formed during freezing and the induced porous microstructure consists of uniform small pores. At higher freezing temperature and lower average cooling rate, the opposite trend could take place. Ice crystal growth is more kinetically favoured than ice nucleation [138]. Therefore, a small number of large ice crystals are probably formed during freezing. These results show that the control of the solidification conditions through the applied temperature gradient and cooling rate prior to freeze-drying is crucial in "building" the final microstructure of nanocellulose foams.

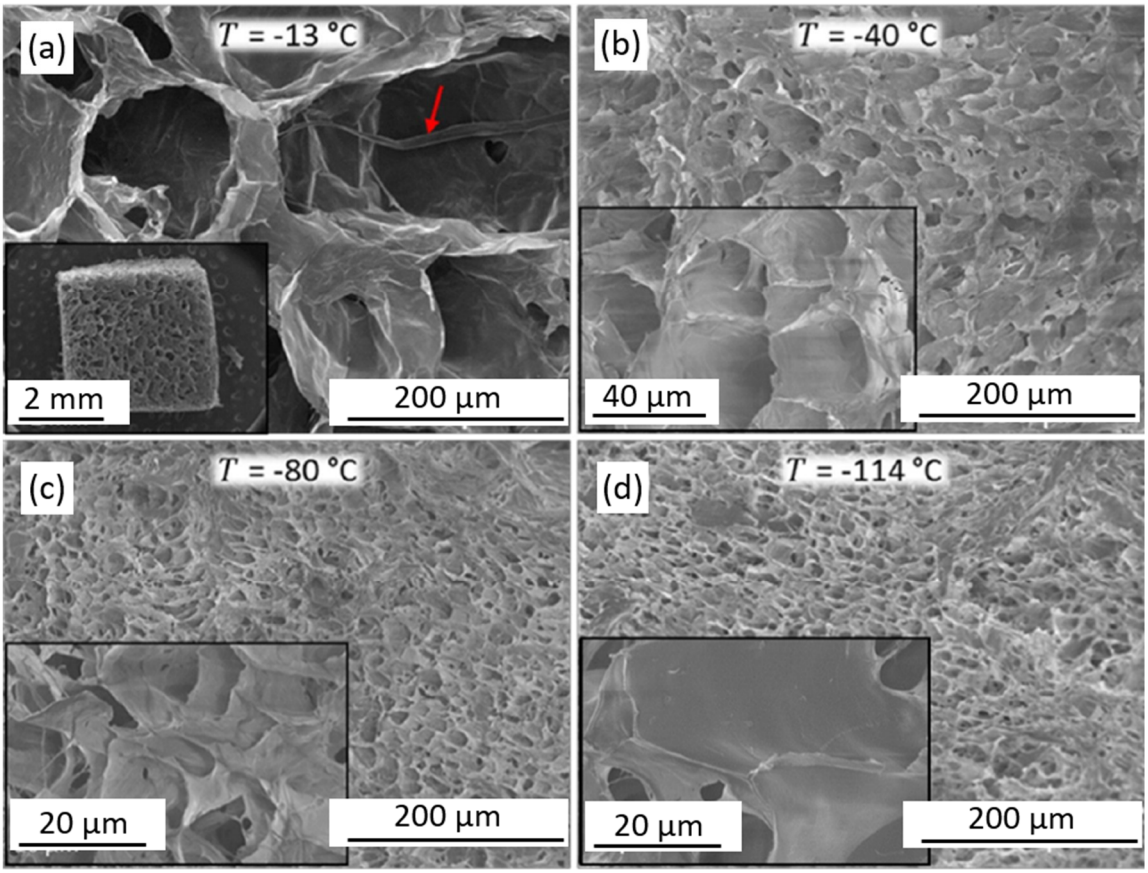

Figure 11. SEM micrographs of CNF foams obtained after freezing at various temperatures and then sublimation. The images inset are SEM micrographs of CNF foams obtained at lower (**a**) or higher (**b**–**d**) magnifications (Adapted from Martoïa et al. [56] with permission from Elsevier).

4.2. Effect of the Suspension Formulation

4.2.1. Suspending Fluid

The characteristics and properties of the fluid that is used to disperse the colloids are crucial in the ice-templating process [64–67]. The fluid properties can affect (i) the crystal morphology, (ii) the state of dispersion of the suspended particles, and (iii) the mechanisms of particle segregation and redistribution occurring during the solidification phase. If these phenomena and their effects on the final microstructures have been investigated for many ice-templating systems, much less is known concerning nanocellulose systems.

Sehaqui et al. [139] produced thin nanoporous membranes (Figure 12a) from CNF dispersions in ter-buthyl alcohol (TBA). Aqueous CNF suspensions were completely solvent exchanged to TBA through ethanol. The CNF membranes that were obtained after freezing and sublimation showed fine porous microstructures with nanometric pore sizes (average pore size of about 24 nm) and also the presence of domains with aggregated CNFs. Nemato et al. [140] also produced thin nanoporous filter membranes using TBA. However, in that study, CNFs were dispersed in various water/TBA mixtures at TBA concentrations up to 60 wt% before freezing at T ≈ -20 °C and sublimation. Interestingly, the authors observed that the materials prepared without adding TBA exhibited columnar structures with micrometer-sized large pores, whereas those obtained from CNF dispersions in water/TBA mixtures at TBA concentrations ranging from 20 to 50 wt% displayed fine porous structures, in the form of CNF networks, with nanometer-sized fine pores (Figure 12b). In contrast, the CNF filters prepared from CNF/water/TBA dispersions with 60 wt% TBA showed heterogeneous microstructures with large pores and film-like structures together with fine porous structures. The role of TBA in the formation

of fine porous structures after ice-templating can be related to the two following scenarios. Firstly, the presence of TBA molecules in water changes the morphology and growth kinetics of ice-crystals. A finer analysis of the phase diagram of the binary mixture of water/TBA reveals that two eutectic compositions exists, respectively, on the water-rich and TBA-rich sides of the phase diagram [141]. In addition, various TBA hydrates can also be formed, depending on the TBA concentration and freezing temperature [141]. Hence, a wide diversity of crystal morphologies can be observed during the solidification of a binary mixture of water/TBA [142]. Secondly, TBA molecules can attach to the surface of CNFs through hydrogen-bonding interactions which leads to hydrophobic surfaces of the fibrils by introducing tert-butyl groups [143]. This can considerably disturb the redistribution of solid particles by the solidification front. Indeed, the chemical steric hindrance effect of the tert-butyl groups can restrict the self-association behaviour of CNFs and the formation of continuous cell walls as well. It is also worth noting that the addition of TBA can disturb the colloidal stability of nanocellulose systems. This last point is presumably at the origin of the heterogeneous porous microstructures observed by Nemoto et al. [140] for filters prepared with 60 wt% TBA (Figure 12b). The effect of the colloidal stability on the microstructure of ice-templated materials is discussed further in the next subsection.

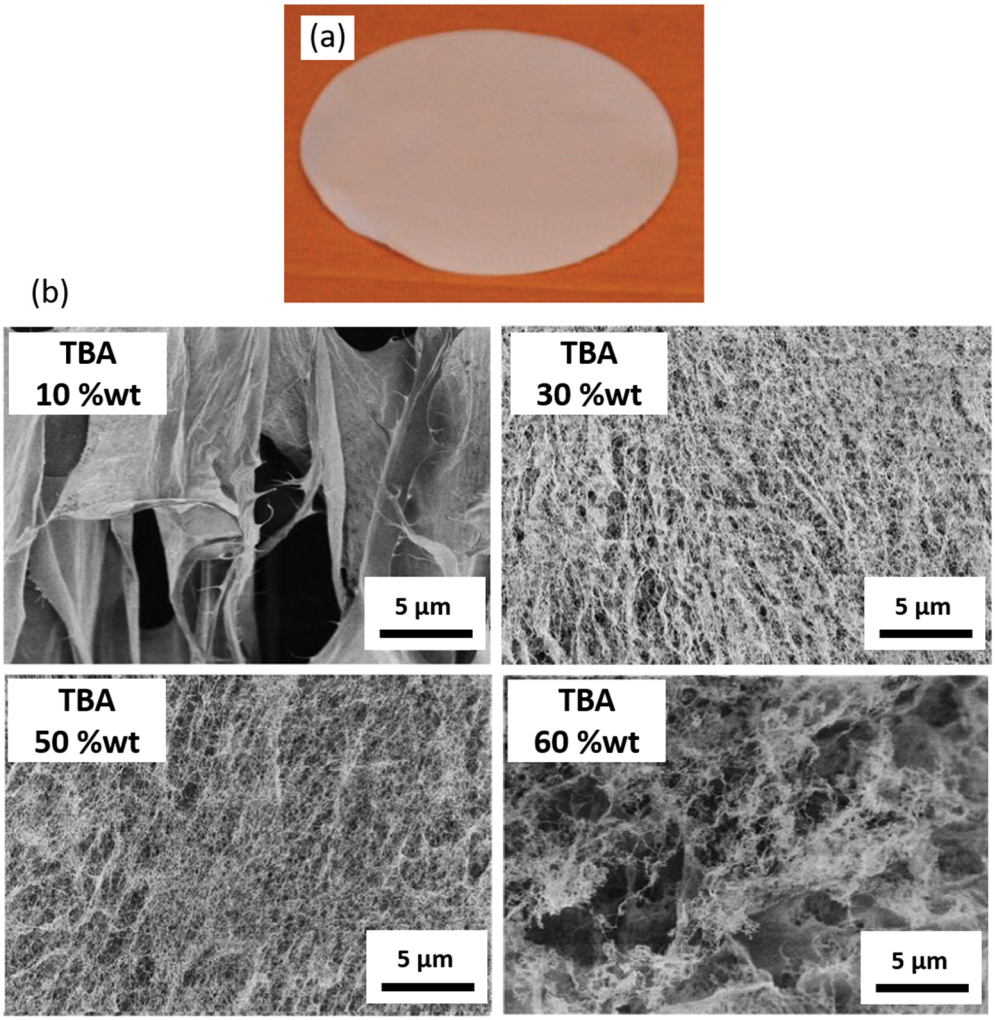

Figure 12. (**a**) Photograph of a porous CNF film of high specific surface area obtained after freezing a CNF dispersion in ter-buthyl-alcohol (TBA) and then sublimation. (Adapted with permission from Sehaqui et al. [139]. Copyright 2011 American Chemical Society). (**b**) SEM micrographs of CNF filters obtained from various CNF/water/TBA dispersions with 0–60 wt% TBA. (Adapted with permission from Nemoto et al. [140]. Copyright 2015 American Chemical Society).

4.2.2. Colloidal Stability of Nanocellulose Suspensions

Electrostatic stabilisation is the main mechanism for stabilisation of cellulose nanoparticles against aggregation and flocculation [90,92]. The colloidal stability of nanocellulose suspensions depends on the chosen extraction processing route that confers to CNFs or CNCs different surface charge density [18,26]. The destabilisation of nanocellulose suspension is also often accomplished by the addition of salt or changing the pH to effectively neutralise or screen the (repulsive) surface charge of the particles [90,91,144,145]. Martoïa et al. [56] investigated the effect of the CNF type on the resulting microstructures of ice-templated foams. The authors prepared CNF foams using two types of CNF suspensions, namely enzymatic and TEMPO-oxidised CNF suspensions. Enzymatic CNF suspensions exhibited spatially heterogeneous mesostructures such as flocs (50–100 µm). In contrast, TEMPO-oxidised CNF suspensions were electrostatically stabilised suspensions and thus did not exhibit flocculated textures. Noticeable structural differences between enzymatic and TEMPO-oxidised CNF foams were observed. As shown in Figure 13, the geometry of TEMPO-oxidised cell foams was much more regular compared with that of enzymatic foams. These observations show the role of the colloidal stability of nanocellulose suspensions on the phenomena of particle segregation, entrapment, and redistribution that occur during ice growth. Because of their strongest colloidal stability, TEMPO-oxidised CNFs are presumably more homogenously redistributed by the moving ice front, leading to more regular structures [56]. The situation is probably more complex and chaotic with enzymatic suspensions since they are more polydisperse, less stable and thus exhibit mesoscale heterogeneities in the form of flocs or floc chains. These flocs could be encapsulated or torn by the moving ice front, instead of being homogeneously redistributed. These complex mechanisms are potentially at the origin of the structural defects and heterogeneities, such as the numerous dangling masses and torn cell walls (Figure 13).

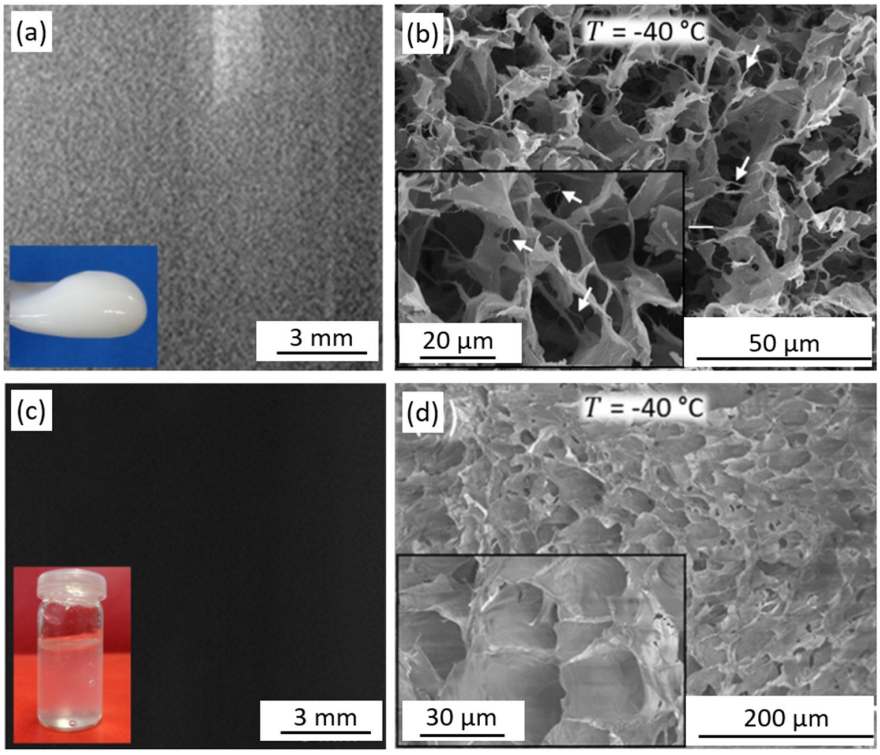

Figure 13. Photographs obtained with a black background of a 2-wt% enzymatic CNF suspension (**a**), and a 0.75-wt% TEMPO-oxidised CNF suspension (**c**). SEM micrographs of enzymatic CNF foams ($\rho \simeq 23$ kg m^{-3}) (**b**) and TEMPO-oxidised CNF foams ($\rho \simeq 11$ kgm^{-3}) (**d**). (Adapted from Martoïa et al. [56] with permission from Elsevier).

4.2.3. Nanocellulose Concentration

Sehaqui et al. [40,146] and Martoïa et al. [56] investigated the effect of the CNF concentration on the microstructures of ice-templated foams. Both studies showed that the foam pore size decreased with increasing the CNF concentration (Figure 14). Using gas absorption experiments, Munier et al. [120] also observed that the density of the foam cell walls increased with increasing CNF concentration. The decrease in the foam pore size could be related to the increase with the CNF concentration in the rheological properties of the suspensions, namely the yield stress τ_0 [100]. Higher yield stress would restrain ice crystal growth, so that nucleation sites would be induced, resulting in the formation of numerous small pores.

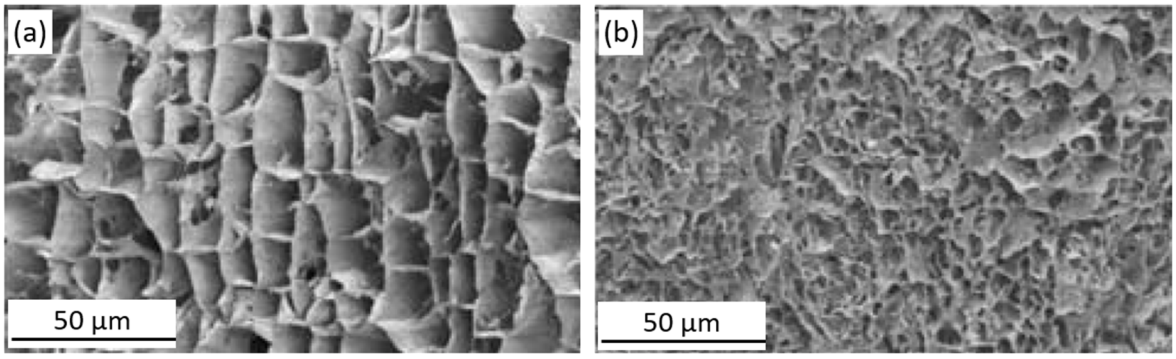

Figure 14. FE-SEM micrographs of the cryo-fractured surface of the CNF foams with a density ρ of (**a**) 7 kg m^{-3} and (**b**) 61 kg m^{-3}. Note that these foams were prepared by direct quenching at a freezing temperature of −196 °C. (Adapted from Sehaqui et al. [40] with permission from the Royal Society of Chemistry).

4.2.4. Polymer Additives

The fabrication of ice-templated foams from CNF-water-polymer dispersions has first been done by Svagan et al. [123,147] with the main objective of tuning the mechanical properties of foam cell walls. Several CNF-starch nanocomposite foams were thus prepared by varying the starch content from 30 to 100 wt%. The authors observed that the addition of solubilised starch had a significant effect not only on the mechanical performances of the foams but also on the pore morphologies. Smaller cells, larger anisotropy ratios and more closed cells were observed with higher starch contents [147]. It was assumed that the presence of starch in the CNF suspensions affect ice crystal growth. The effect of starch would be to (i) promote ice nucleation and (ii) slow down the average kinetic of ice crystals growth by decreasing the diffusion rate of water molecules to the growing crystal surface.

More recently, Chau et al. [148] used polymer additives to obtain CNC foams with tunable porous microstructures. The authors added hydrazide-functionalised poly(oligoethylene glycol methacrylate) (H-POEGMA) to CNC suspensions. In order to obtain a chemical cross-linking between CNCs and H-POEGMA, the surface hydroxyl groups of cellulose nanocrystals was also selectively oxidised to aldehyde groups [149]. In doing so, the authors showed that by controlling the composition of the CNC/H-POEGMA dispersions, foams with fibrillary, columnar, or lamellar pore morphologies were produced (Figure 15). However, the chemical, physical, and mechanical phenomena involved are still not fully elucidated.

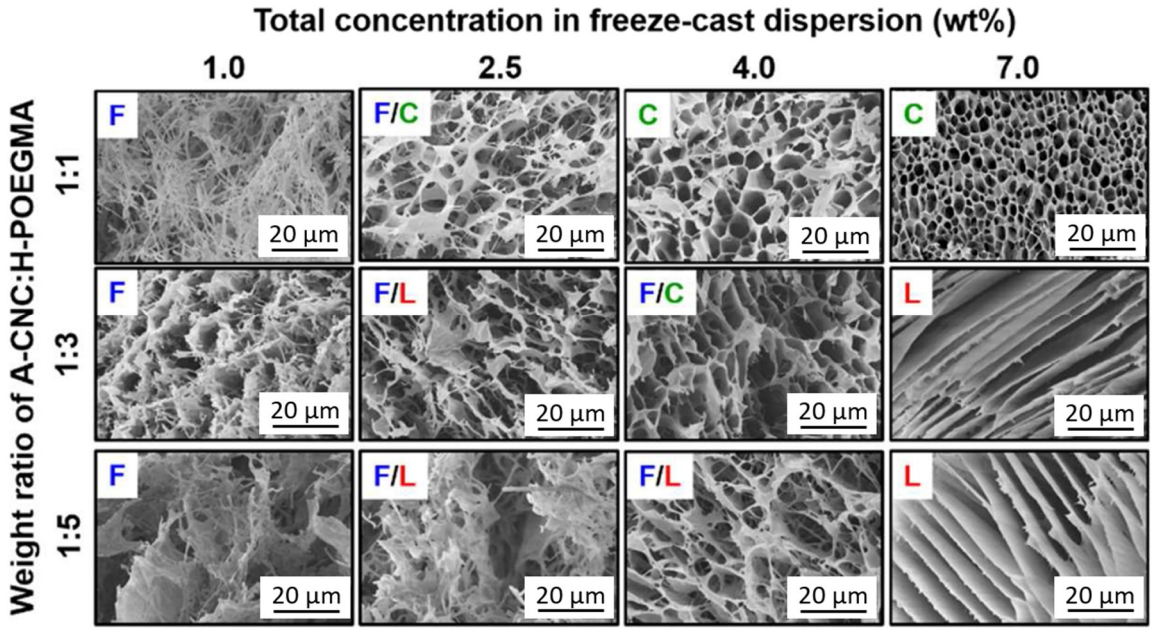

Figure 15. SEM micrographs of CNC foams' cross-sections (perpendicular to the ice growth direction) showing the various pore morphologies that can be obtained depending on both the amount of added hydrazide-functionalised poly(oligoethylene glycol methacrylate) H-POEGMA and CNC concentration. (Adapted with permission from Chau et al. [148]. Copyright 2016 American Chemical Society).

4.2.5. Nanofibre Slenderness

The nanofibre slenderness $r = l/d$ was shown to have a significant effect on the foam shrinkage. As previously mentioned, Martoïa et al. [56] observed that the foam shrinkage increased drastically when C_i was lower than a critical concentration C*. This critical concentration C* was found to depend on the nanofibre slenderness r and colloidal interactions between the particles [56,100]. Using volume excluded concepts, the authors showed that C* probably corresponded to a percolation threshold below which nanocellulose networks were no longer connected and lost their mechanical integrity. The percolation threshold that corresponds to a critical number of bonds or interactions per nanofibre z^*, was estimated using the statistical tube model for fibrous networks of homogeneously distributed straight fibres [150–152]:

$$z^* = 4\phi^* \left(\frac{2}{\pi} r\Phi_1 + \Phi_2 + 1 \right) \approx 2 \quad (1)$$

where ϕ^* is the critical nanofibre volume content and Φ_1, Φ_2 are the orientation distribution functions ($\Phi_1 = \pi/4$ and $\Phi_2 = 1/2$ for isotropic fibrous microstructures [150]). Using this analytical estimate, the authors found that $z^* \approx 2$. Below z^*, particle depletion or migration phenomena that are induced by ice formation could be facilitated, in particular near the sample external surface [56].

Further, the morphology of the pores/cells can also vary significantly with the nanofibre slenderness. Munier et al. [120] prepared ice-templated foams using two types of electrostatically stabilised nanocellulose suspensions, namely an aqueous suspension of long and slender CNFs ($r \approx 100$) (Figure 16a) and a suspension of CNCs with much lower aspect ratio ($r \approx 35$) (Figure 16b). Interestingly, the authors observed that the suspensions of slender CNFs lead to foams with tubular-like porous structures (Figure 16c), whereas foams produced from the shorter and more rigid CNCs displayed lamellar porous structures (Figure 16d). The difference in pore morphology could be related to the ability of CNFs to entangle and form highly connected and cohesive fibrous networks that would restrain the growth of large, lamellar ice crystals.

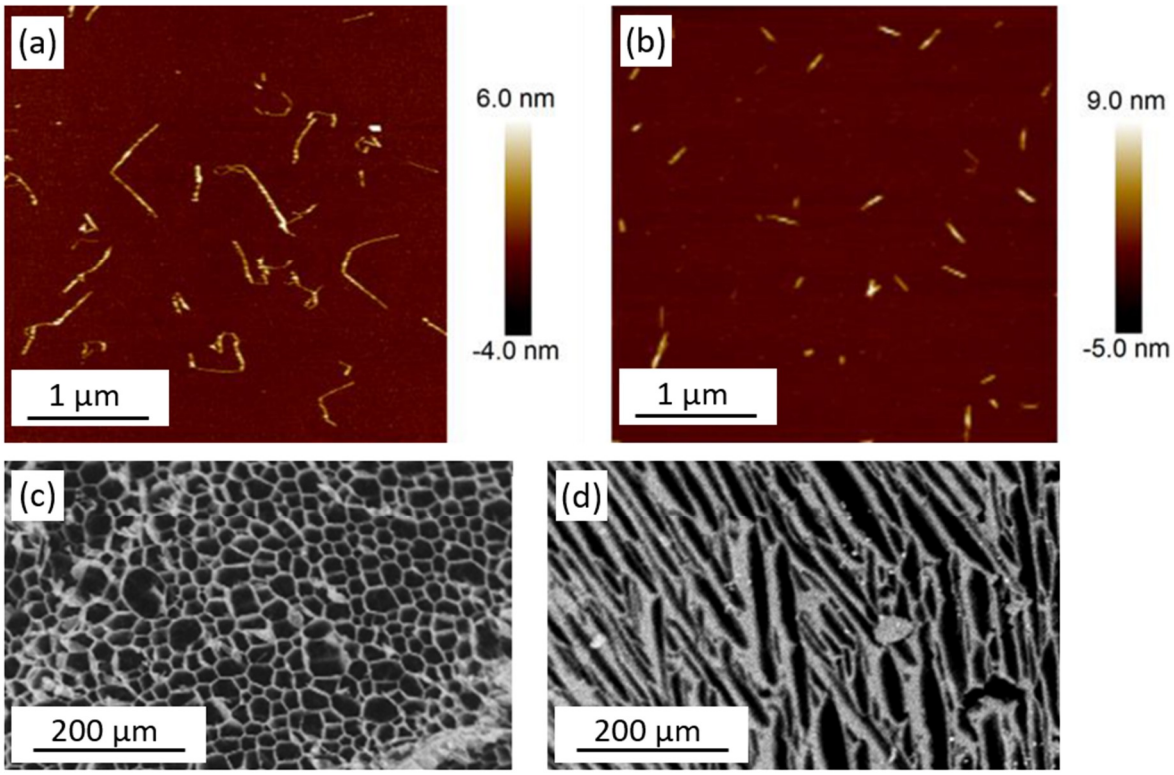

Figure 16. AFM images of CNFs (**a**) and CNCs (**b**). The nanocellulose particles are electrostatically adsorbed onto cationised mica substrates. The magnification is the same in both images and the scale bar is 500 nm. SEM micrographs of CNF (**c**,**d**) CNC foams obtained by ice-templating from a 0.5 wt% CNF suspension and a 1.5 wt% CNC suspension, respectively. (Adapted with permission from Munier et al. [120]. Copyright 2016 American Chemical Society).

4.3. Effect on the End-Use Properties

As shown in the previous sections, ice-templated nanocellulose-based materials can exhibit a wide variety of microstructures, depending on the choice of the nanocellulose suspension, their formulation, and the processing conditions. Ice-templated materials can have medium to high porosity ε ($80\% \leq \varepsilon \leq 99\%$), cellular, tubular, or lamellar structures with nano- and/or micro-sized pores (average pore size ranging from 0.1 µm to 800 µm). Obtaining materials with tailored microstructures is of great interest for materials engineering owing to the broad diversity of performances that these materials can exhibit. Indeed, the physical and mechanical properties of porous materials can vary widely, depending on the choice of the solid from which they are made, the volume fraction of the solid ϕ, and the geometry of the pores/cells [43]. For instance, Sehaqui et al. [40] investigated the effect of the density ρ (or porosity) on the compression properties of CNF foams. The authors observed that the compression modulus E and the yield stress σ_y of the foams increased from 56 to 5310 kPa and 8 to 516 kPa with increasing the density ρ from 7 to 103 kg m^{-3}. Martoïa et al. [56] also investigated the effect of the density ρ on the compression behaviour of CNF foams. Both the compression modulus E and the yield stress σ_y were found to be power-law functions of the volume fraction of solid ϕ, i.e.; $E \propto \phi^n$ and $\sigma_y \propto \phi^m$. However, the authors observed that the values of n and m were affected by the foam architecture, namely the regularity and geometry of the cells. The scaling exponents ($n = 2.29$ and $m = 2.22$) of TEMPO-oxidised CNF foams were close to those expected for classical cellular materials with well-defined microstructures and deformation mechanisms such as open ($n = 2$ and $m = 1.5$) or closed foams without thickening of edges ($n = 3$ and $m = 2$) [43,56]. In contrast, the scaling exponents ($n = 3.11$ and $m = 3.04$) of enzymatic CNF foams were close to those usually obtained for aerogels [44,153], i.e., $3 < n < 4$ and $2.5 < m < 3.5$. This behavior could be related to the disordered

cellular structure of these foams and more precisely to the existence of numerous dangling masses or branches that hung off the cell walls [153,154].

Ice-templated materials are also widely studied owing to their high thermal insulation properties. As for the mechanics, thermal properties vary with the density and the microstructural features of porous materials [43]. Jiménez-Saelices et al. [119] observed that the apparent thermal conductivity λ of CNF foams with quasi-isotropic cellular microstructures increased from 38 to 43 mW $m^{-1}K^{-1}$ with increasing the density ρ from 12 to 43 kg m^{-3}. Wicklein et al. [41] produced CNF foams of density ρ = 5.6 kg m^{-3} with anisotropic tubular porous microstructures. The authors reported that the thermal conductivity λ measured in the axial direction (along the pore) was close to 170 mW $m^{-1}K^{-1}$, whereas those measured in the radial direction was significantly lower, i.e., close to 15 mW m^{-1} K^{-1}. These examples emphasise the undeniable role of the porous architecture on the resulting performances of nanocellulose-based materials. The selection and the use of a specific material for a particular engineering application require a proper control of the porous microstructure to reach the physical and/or mechanical performances required for specific applications. A more complete description of the physical and mechanical properties of porous nanocellulose-based materials can be found in the following references [52,85].

5. Conclusions and Outlook

Many forming processes using the principle of ice-templating have been developed to obtain porous materials from nanocellulose dispersions. These processing routes commonly involve two main steps: (i) the preparation of the nanocellulose suspension and (ii) the solidification and removal of the suspending fluid by lyophilisation. Depending on the chosen process, nanocellulose-based materials with varied shapes and structures can be manufactured such as semi-structural foam panels, microbeads, filter membranes, and scaffolds. The fabrication methods are also versatile enough to tune easily the process-induced microstructures. A large number of factors related both to the processing conditions (e.g., temperature gradient, cooling rate) and the nature of colloids (particles, size, surface charge density, conductivity, addition of salt or polymer, etc.) can be used to achieve complex and customisable architectures suited for target application requirements. Ice-templated nanocellulose-based materials can exhibit a broad diversity of physical (thermal, acoustic, permeation, etc.) and mechanical properties owing to their tunable microstructure. These materials can exhibit medium to high porosity ε ($80\% \leq \varepsilon \leq 99\%$), varied pore morphology (tubular, cellular, and lamellar), and a pore size distribution defined at several length scales (from the nanoscale to the millimetre scale). In addition, the processes using the principle of ice-templating are almost material agnostic, i.e., almost any type of materials can be used. As such, multifunctional porous nanocellulose-based materials can also be designed by combining CNCs or CNFs with polymers [137,147,155] or other nanoscale particles such as carbon nanotubes [156,157], graphene [158], and silver nanoparticles [159]. Ice-templated nanocellulose-based materials constitutes promising biobased solutions for a wide diversity of engineering fields including construction, transportation, energy, and biomedical sectors.

However, the existing manufacturing processes still suffer from important limitations related both to the inherent characteristics of nanocellulose suspensions and the ice-templating technique. Nanocelluloses are colloidal fibrous systems that exhibit a complex rheology between that of soft solids and liquids. These suspensions are thus difficult to use in forming processes, particularly in concentrated regimes. Extensive research should be carried out in order to better characterise and understand the rheology of nanocellulose suspensions in concentrated and hyper-concentrated regimes. Then, the existing processes are multi-step processes with long production cycles. In particular, the freeze-drying or lyophilisation phase is time-consuming and research efforts are still required to make this step more efficient. For instance, additives or solvents with low enthalpy of sublimation could be used to increase the sublimation kinetics. In addition, the control of the temperature gradient during the processing of the materials still need to be improved. Most of ice-templated materials exhibit core-shell architectures, microstructure gradients and anisotropic pore morphologies. They

also exhibit heterogeneities and numerous structural defects such as dangling masses and torn cell walls. These defects significantly reduce the physical and mechanical properties of ice-templated materials [56]. Research efforts must be done to better characterise and understand the phenomena involved in the formation of foam cells [160–162] as well as those related to the shrinkage of materials during solidification and freeze-drying of nanocellulose suspensions.

Author Contributions: Conceptualization, S.G., F.M., L.O. and P.J.J.D.; writing—original draft preparation, S.G., F.M., L.O. and P.J.J.D.; writing—review and editing, S.G., F.M., L.O. and P.J.J.D.; supervision, F.M., L.O. and P.J.J.D.; project administration, F.M., L.O. and P.J.J.D.; funding acquisition, F.M., L.O. and P.J.J.D.

Funding: This research was supported by IDEX Université Grenoble Alpes. The authors gratefully acknowledge LabEX Tec 21 and the research site of INSA Lyon at Oyonnax for administrative and technical support.

Conflicts of Interest: The authors declare no conflict of interest. The funders had no role in the design of the study; in the collection, analyses, or interpretation of data; in the writing of the manuscript, or in the decision to publish the results.

References

1. Moon, R.J.; Martini, A.; Nairn, J.; Simonsen, J.; Youngblood, J. Cellulose nanomaterials review: Structure, properties and nanocomposites. *Chem. Soc. Rev.* **2011**, *40*, 3941–3994. [CrossRef] [PubMed]
2. Klemm, D.; Heublein, B.; Fink, H.P.; Bohn, A. Cellulose: Fascinating Biopolymer and Sustainable Raw Material. *Angew. Chem. Int. Ed.* **2005**, *44*, 3358–3393. [CrossRef] [PubMed]
3. Gibson, L.J. The hierarchical structure and mechanics of plant materials. *J. R. Soc. Interface* **2012**, rsif20120341. [CrossRef] [PubMed]
4. Niklas, K.J. *Plant Biomechanics: An Engineering Approach to Plant Form and Function*; University of Chicago Press: Chicago, IL, USA, 1992; ISBN 978-0-226-58631-1.
5. Klemm, D.; Cranston, E.D.; Fischer, D.; Gama, M.; Kedzior, S.A.; Kralisch, D.; Kramer, F.; Kondo, T.; Lindström, T.; Nietzsche, S.; et al. Nanocellulose as a natural source for groundbreaking applications in materials science: Today's state. *Mater. Today* **2018**, *21*, 720–748. [CrossRef]
6. Habibi, Y.; Lucia, L.A.; Rojas, O.J. Cellulose Nanocrystals: Chemistry, Self-Assembly, and Applications. *Chem. Rev.* **2010**, *110*, 3479–3500. [CrossRef] [PubMed]
7. Varshney, V.K.; Naithani, S. Chemical Functionalization of Cellulose Derived from Nonconventional Sources. In *Cellulose Fibers: Bio- and Nano-Polymer Composites: Green Chemistry and Technology*; Kalia, S., Kaith, B.S., Kaur, I., Eds.; Springer: Berlin/Heidelberg, Germany, 2011; pp. 43–60, ISBN 978-3-642-17370-7.
8. Siró, I.; Plackett, D. Microfibrillated cellulose and new nanocomposite materials: A review. *Cellulose* **2010**, *17*, 459–494. [CrossRef]
9. Stelte, W.; Sanadi, A.R. Preparation and Characterization of Cellulose Nanofibers from Two Commercial Hardwood and Softwood Pulps. *Ind. Eng. Chem. Res.* **2009**, *48*, 11211–11219. [CrossRef]
10. Fernandes, A.N.; Thomas, L.H.; Altaner, C.M.; Callow, P.; Forsyth, V.T.; Apperley, D.C.; Kennedy, C.J.; Jarvis, M.C. Nanostructure of cellulose microfibrils in spruce wood. *PNAS* **2011**. [CrossRef] [PubMed]
11. Ciesielski, P.N.; Matthews, J.F.; Tucker, M.P.; Beckham, G.T.; Crowley, M.F.; Himmel, M.E.; Donohoe, B.S. 3D Electron Tomography of Pretreated Biomass Informs Atomic Modeling of Cellulose Microfibrils. *ACS Nano* **2013**, *7*, 8011–8019. [CrossRef] [PubMed]
12. Larsson, P.T.; Wickholm, K.; Iversen, T. A CP/MAS13C NMR investigation of molecular ordering in celluloses. *Carbohydr. Res.* **1997**, *302*, 19–25. [CrossRef]
13. Usov, I.; Nyström, G.; Adamcik, J.; Handschin, S.; Schütz, C.; Fall, A.; Bergström, L.; Mezzenga, R. Understanding nanocellulose chirality and structure–properties relationship at the single fibril level. *Nat. Commun.* **2015**, *6*, 7564. [CrossRef] [PubMed]
14. Donaldson, L. Cellulose microfibril aggregates and their size variation with cell wall type. *Wood Sci. Technol.* **2007**, *41*, 443. [CrossRef]
15. Chinga-Carrasco, G. Cellulose fibres, nanofibrils and microfibrils: The morphological sequence of MFC components from a plant physiology and fibre technology point of view. *Nanoscale Res. Lett.* **2011**, *6*, 417. [CrossRef] [PubMed]

16. Martoïa, F.; Perge, C.; Dumont, P.J.J.; Orgéas, L.; Fardin, M.A.; Manneville, S.; Belgacem, M.N. Heterogeneous flow kinematics of cellulose nanofibril suspensions under shear. *Soft Matter* **2015**, *11*, 4742–4755. [CrossRef] [PubMed]
17. Saito, T.; Kimura, S.; Nishiyama, Y.; Isogai, A. Cellulose Nanofibers Prepared by TEMPO-Mediated Oxidation of Native Cellulose. *Biomacromolecules* **2007**, *8*, 2485–2491. [CrossRef] [PubMed]
18. Isogai, A.; Saito, T.; Fukuzumi, H. TEMPO-oxidized cellulose nanofibers. *Nanoscale* **2011**, *3*, 71–85. [CrossRef] [PubMed]
19. Jorfi, M.; Foster, E.J. Recent advances in nanocellulose for biomedical applications. *J. Appl. Polym. Sci.* **2015**, *132*. [CrossRef]
20. Dufresne, A. *Nanocellulose: From Nature to High Performance Tailored Materials*; Walter de Gruyter GmbH & Co KG: Berlin, Germany, 2017; ISBN 978-3-11-048041-2.
21. Henriksson, M.; Henriksson, G.; Berglund, L.A.; Lindström, T. An environmentally friendly method for enzyme-assisted preparation of microfibrillated cellulose (MFC) nanofibers. *Eur. Polym. J.* **2007**, *43*, 3434–3441. [CrossRef]
22. Pääkkö, M.; Ankerfors, M.; Kosonen, H.; Nykänen, A.; Ahola, S.; Österberg, M.; Ruokolainen, J.; Laine, J.; Larsson, P.T.; Ikkala, O.; et al. Enzymatic Hydrolysis Combined with Mechanical Shearing and High-Pressure Homogenization for Nanoscale Cellulose Fibrils and Strong Gels. *Biomacromolecules* **2007**, *8*, 1934–1941. [CrossRef] [PubMed]
23. Wågberg, L.; Decher, G.; Norgren, M.; Lindström, T.; Ankerfors, M.; Axnäs, K. The Build-Up of Polyelectrolyte Multilayers of Microfibrillated Cellulose and Cationic Polyelectrolytes. *Langmuir* **2008**, *24*, 784–795. [CrossRef] [PubMed]
24. Beck-Candanedo, S.; Roman, M.; Gray, D.G. Effect of Reaction Conditions on the Properties and Behavior of Wood Cellulose Nanocrystal Suspensions. *Biomacromolecules* **2005**, *6*, 1048–1054. [CrossRef] [PubMed]
25. Abdul Khalil, H.P.S.; Davoudpour, Y.; Islam, M.N.; Mustapha, A.; Sudesh, K.; Dungani, R.; Jawaid, M. Production and modification of nanofibrillated cellulose using various mechanical processes: A review. *Carbohydr. Polym.* **2014**, *99*, 649–665. [CrossRef] [PubMed]
26. Nechyporchuk, O.; Belgacem, M.N.; Bras, J. Production of cellulose nanofibrils: A review of recent advances. *Ind. Crops Prod.* **2016**, *93*, 2–25. [CrossRef]
27. Brinchi, L.; Cotana, F.; Fortunati, E.; Kenny, J.M. Production of nanocrystalline cellulose from lignocellulosic biomass: Technology and applications. *Carbohydr. Polym.* **2013**, *94*, 154–169. [CrossRef] [PubMed]
28. Kargarzadeh, H.; Ahmad, I.; Thomas, S.; Dufresne, A. *Handbook of Nanocellulose and Cellulose Nanocomposites*; John Wiley & Sons: Hoboken, NJ, USA, 2017; ISBN 978-3-527-68998-9.
29. Kontturi, E.; Laaksonen, P.; Linder, M.B.; Gröschel, A.H.; Rojas, O.J.; Ikkala, O. Advanced Materials through Assembly of Nanocelluloses. *Adv. Mater.* **2018**, *30*, 1703779. [CrossRef] [PubMed]
30. Dufresne, A. Cellulose nanomaterials as green nanoreinforcements for polymer nanocomposites. *Philos. Trans. R. Soc. A* **2018**, *376*, 20170040. [CrossRef] [PubMed]
31. Benítez, A.J.; Walther, A. Cellulose nanofibril nanopapers and bioinspired nanocomposites: A review to understand the mechanical property space. *J. Mater. Chem. A* **2017**, *5*, 16003–16024. [CrossRef]
32. Mariano, M.; Kissi, N.E.; Dufresne, A. Cellulose nanocrystals and related nanocomposites: Review of some properties and challenges. *J. Polym. Sci. Part B Polym. Phys.* **2014**, *52*, 791–806. [CrossRef]
33. Larsson, P.A.; Berglund, L.A.; Wågberg, L. Ductile All-Cellulose Nanocomposite Films Fabricated from Core–Shell Structured Cellulose Nanofibrils. *Biomacromolecules* **2014**, *15*, 2218–2223. [CrossRef] [PubMed]
34. Bardet, R.; Belgacem, N.; Bras, J. Flexibility and Color Monitoring of Cellulose Nanocrystal Iridescent Solid Films Using Anionic or Neutral Polymers. *ACS Appl. Mater. Interfaces* **2015**, *7*, 4010–4018. [CrossRef] [PubMed]
35. Håkansson, K.M.O.; Fall, A.B.; Lundell, F.; Yu, S.; Krywka, C.; Roth, S.V.; Santoro, G.; Kvick, M.; Prahl Wittberg, L.; Wågberg, L.; et al. Hydrodynamic alignment and assembly of nanofibrils resulting in strong cellulose filaments. *Nat. Commun.* **2014**, *5*, 4018. [CrossRef] [PubMed]
36. Mittal, N.; Ansari, F.; Gowda, V.K.; Brouzet, C.; Chen, P.; Larsson, P.T.; Roth, S.V.; Lundell, F.; Wågberg, L.; Kotov, N.A.; et al. Multiscale Control of Nanocellulose Assembly: Transferring Remarkable Nanoscale Fibril Mechanics to Macroscale Fibers. *ACS Nano* **2018**, *12*, 6378–6388. [CrossRef] [PubMed]

37. Kobayashi, Y.; Saito, T.; Isogai, A. Aerogels with 3D Ordered Nanofiber Skeletons of Liquid-Crystalline Nanocellulose Derivatives as Tough and Transparent Insulators. *Angew. Chem. Int. Ed.* **2014**, *53*, 10394–10397. [CrossRef] [PubMed]
38. Yang, X.; Shi, K.; Zhitomirsky, I.; Cranston, E.D. Cellulose Nanocrystal Aerogels as Universal 3D Lightweight Substrates for Supercapacitor Materials. *Adv. Mater.* **2015**, *27*, 6104–6109. [CrossRef] [PubMed]
39. Heath, L.; Thielemans, W. Cellulose nanowhisker aerogels. *Green Chem.* **2010**, *12*, 1448–1453. [CrossRef]
40. Sehaqui, H.; Salajková, M.; Zhou, Q.; Berglund, L.A. Mechanical performance tailoring of tough ultra-high porosity foams prepared from cellulose I nanofiber suspensions. *Soft Matter* **2010**, *6*, 1824–1832. [CrossRef]
41. Wicklein, B.; Kocjan, A.; Salazar-Alvarez, G.; Carosio, F.; Camino, G.; Antonietti, M.; Bergström, L. Thermally insulating and fire-retardant lightweight anisotropic foams based on nanocellulose and graphene oxide. *Nat. Nanotechnol.* **2015**, *10*, 277–283. [CrossRef] [PubMed]
42. Gupta, P.; Singh, B.; Agrawal, A.K.; Maji, P.K. Low density and high strength nanofibrillated cellulose aerogel for thermal insulation application. *Mater. Des.* **2018**, *158*, 224–236. [CrossRef]
43. Gibson, L.J.; Ashby, M.F. *Cellular Solids: Structure and Properties*; Cambridge University Press: Cambridge, UK, 1999; ISBN 978-0-521-49911-8.
44. Hüsing, N.; Schubert, U. Aerogels—Airy Materials: Chemistry, Structure, and Properties. *Angew. Chem. Int. Ed.* **1998**, *37*, 22–45. [CrossRef]
45. Fricke, J. Aerogels—A Fascinating Class of High-Performance Porous Solids. In *Aerogels*; Fricke, J., Ed.; Springer Proceedings in Physics; Springer: Berlin/Heidelberg, Germany, 1986; pp. 2–19.
46. Aulin, C.; Netrval, J.; Wågberg, L.; Lindström, T. Aerogels from nanofibrillated cellulose with tunable oleophobicity. *Soft Matter* **2010**, *6*, 3298–3305. [CrossRef]
47. Srinivasa, P.; Kulachenko, A.; Aulin, C. Experimental characterisation of nanofibrillated cellulose foams. *Cellulose* **2015**, *22*, 3739–3753. [CrossRef]
48. Srinivasa, P.; Kulachenko, A. Analysis of the compressive response of Nano Fibrillar Cellulose foams. *Mech. Mater.* **2015**, *80*, 13–26. [CrossRef]
49. Srinivasa, P.; Kulachenko, A.; Karlberg, F. Material properties of the cell walls in nanofibrillar cellulose foams from finite element modelling of tomography scans. *Cellulose* **2017**, *24*, 519–533. [CrossRef]
50. Lin, N.; Dufresne, A. Nanocellulose in biomedicine: Current status and future prospect. *Eur. Polym. J.* **2014**, *59*, 302–325. [CrossRef]
51. Miyamoto, T.; Takahashi, S.; Ito, H.; Inagaki, H.; Noishiki, Y. Tissue biocompatibility of cellulose and its derivatives. *J. Biomed. Mater. Res.* **1989**, *23*, 125–133. [CrossRef] [PubMed]
52. Lavoine, N.; Bergström, L. Nanocellulose-based foams and aerogels: Processing, properties, and applications. *J. Mater. Chem. A* **2017**, *5*, 16105–16117. [CrossRef]
53. Cervin, N.T.; Andersson, L.; Ng, J.B.S.; Olin, P.; Bergström, L.; Wågberg, L. Lightweight and Strong Cellulose Materials Made from Aqueous Foams Stabilized by Nanofibrillated Cellulose. *Biomacromolecules* **2013**, *14*, 503–511. [CrossRef] [PubMed]
54. Cervin, N.T.; Johansson, E.; Benjamins, J.-W.; Wågberg, L. Mechanisms Behind the Stabilizing Action of Cellulose Nanofibrils in Wet-Stable Cellulose Foams. *Biomacromolecules* **2015**, *16*, 822–831. [CrossRef] [PubMed]
55. Sakai, K.; Kobayashi, Y.; Saito, T.; Isogai, A. Partitioned airs at microscale and nanoscale: Thermal diffusivity in ultrahigh porosity solids of nanocellulose. *Sci. Rep.* **2016**, *6*, 20434. [CrossRef] [PubMed]
56. Martoïa, F.; Cochereau, T.; Dumont, P.J.J.; Orgéas, L.; Terrien, M.; Belgacem, M.N. Cellulose nanofibril foams: Links between ice-templating conditions, microstructures and mechanical properties. *Mater. Des.* **2016**, *104*, 376–391. [CrossRef]
57. Ahlrichs, J.L.; White, J.L. Freezing and Lyophilizing Alters the Structure of Bentonite Gels. *Science* **1962**, *136*, 1116–1118. [CrossRef]
58. Fukasawa, J.-I.; Tsujii, K. Higher-order structure formation of ultrafine boehmite particles in sols, gels, and dried materials. *J. Colloid Interface Sci.* **1988**, *125*, 155–161. [CrossRef]
59. Lu, H.; Qu, Z.; Zhou, Y. Preparation and mechanical properties of dense polycrystalline hydroxyapatite through freeze-drying. *J. Mater. Sci. Mater. Med.* **1998**, *9*, 583–587. [CrossRef] [PubMed]
60. Deville, S. Freeze-Casting of Porous Ceramics: A Review of Current Achievements and Issues. *Adv. Eng. Mater.* **2008**, *10*, 155–169. [CrossRef]

61. Deville, S.; Deville, S. Freeze-Casting of Porous Biomaterials: Structure, Properties and Opportunities. *Materials* **2010**, *3*, 1913–1927. [CrossRef]
62. Deville, S. Ice-templating, freeze casting: Beyond materials processing. *J. Mater. Res.* **2013**, *28*, 2202–2219. [CrossRef]
63. Deville, S. *Freezing Colloids: Observations, Principles, Control, and Use: Applications in Materials Science, Life Science, Earth Science, Food Science, and Engineering*; Springer: Berlin/Heidelberg, Germany, 2017; ISBN 978-3-319-50515-2.
64. Liu, X.; Rahaman, M.N.; Fu, Q. Oriented bioactive glass (13–93) scaffolds with controllable pore size by unidirectional freezing of camphene-based suspensions: Microstructure and mechanical response. *Acta Biomater.* **2011**, *7*, 406–416. [CrossRef] [PubMed]
65. Yoon, B.-H.; Choi, W.-Y.; Kim, H.-E.; Kim, J.-H.; Koh, Y.-H. Aligned porous alumina ceramics with high compressive strengths for bone tissue engineering. *Scr. Mater.* **2008**, *58*, 537–540. [CrossRef]
66. Yang, T.Y.; Lee, J.M.; Yoon, S.Y.; Park, H.C. Hydroxyapatite scaffolds processed using a TBA-based freeze-gel casting/polymer sponge technique. *J. Mater. Sci. Mater. Med.* **2010**, *21*, 1495–1502. [CrossRef] [PubMed]
67. Chen, R.; Wang, C.-A.; Huang, Y.; Ma, L.; Lin, W. Ceramics with Special Porous Structures Fabricated by Freeze-Gelcasting: Using tert-Butyl Alcohol as a Template. *J. Am. Ceram. Soc.* **2007**, *90*, 3478–3484. [CrossRef]
68. Rowe, T.W.G. The theory and practice of freeze-drying. *Ann. N. Y. Acad. Sci.* **1960**, *85*, 641–681. [CrossRef]
69. Fukushima, M.; Yoshizawa, Y. Fabrication of Highly Porous Silica Thermal Insulators Prepared by Gelation–Freezing Route. *J. Am. Ceram. Soc.* **2014**, *97*, 713–717. [CrossRef]
70. Song, H.; Zhao, N.; Qin, W.; Duan, B.; Ding, X.; Wen, X.; Qiu, P.; Ba, X. High-performance ionic liquid-based nanocomposite polymer electrolytes with anisotropic ionic conductivity prepared by coupling liquid crystal self-templating with unidirectional freezing. *J. Mater. Chem. A* **2015**, *3*, 2128–2134. [CrossRef]
71. Fu, Q.; Saiz, E.; Tomsia, A.P. Bioinspired Strong and Highly Porous Glass Scaffolds. *Adv. Funct. Mater.* **2011**, *21*, 1058–1063. [CrossRef] [PubMed]
72. Touri, R.; Moztarzadeh, F.; Sadeghian, Z.; Bizari, D.; Tahriri, M.; Mozafari, M. The Use of Carbon Nanotubes to Reinforce 45S5 Bioglass-Based Scaffolds for Tissue Engineering Applications. Available online: https://www.hindawi.com/journals/bmri/2013/465086/abs/ (accessed on 22 October 2018).
73. Landi, E.; Sciti, D.; Melandri, C.; Medri, V. Ice templating of ZrB2 porous architectures. *J. Eur. Ceram. Soc.* **2013**, *33*, 1599–1607. [CrossRef]
74. Blaker, J.J.; Maquet, V.; Jérôme, R.; Boccaccini, A.R.; Nazhat, S.N. Mechanical properties of highly porous PDLLA/Bioglass® composite foams as scaffolds for bone tissue engineering. *Acta Biomater.* **2005**, *1*, 643–652. [CrossRef] [PubMed]
75. Gouws, G.J.; Shortt, N. Microstructured silver surfaces produced by freeze casting for enhanced phase change heat transfer. *J. Phys. Conf. Ser.* **2015**, *660*, 012045. [CrossRef]
76. Dong, L.; Yang, Q.; Xu, C.; Li, Y.; Yang, D.; Hou, F.; Yin, H.; Kang, F. Facile preparation of carbon nanotube aerogels with controlled hierarchical microstructures and versatile performance. *Carbon* **2015**, *90*, 164–171. [CrossRef]
77. Zhang, X.; Li, C.; Luo, Y. Aligned/Unaligned Conducting Polymer Cryogels with Three-Dimensional Macroporous Architectures from Ice-Segregation-Induced Self-Assembly of PEDOT-PSS. *Langmuir* **2011**, *27*, 1915–1923. [CrossRef] [PubMed]
78. Spender, J.; Demers, A.L.; Xie, X.; Cline, A.E.; Earle, M.A.; Ellis, L.D.; Neivandt, D.J. Method for Production of Polymer and Carbon Nanofibers from Water-Soluble Polymers. *Nano Lett.* **2012**, *12*, 3857–3860. [CrossRef] [PubMed]
79. Röthlisberger, A.; Häberli, S.; Spolenak, R.; Dunand, D.C. Synthesis, structure and mechanical properties of ice-templated tungsten foams. *J. Mater. Res.* **2016**, *31*, 753–764. [CrossRef]
80. Gurauskis, J.; Graves, C.R.; Moreno, R.; Nieto, M.I. Self-supported ceramic substrates with directional porosity by mold freeze casting. *J. Eur. Ceram. Soc.* **2017**, *37*, 697–703. [CrossRef]
81. Moon, Y.W.; Choi, I.J.; Koh, Y.H.; Kim, H.E. Macroporous alumina scaffolds consisting of highly microporous hollow filaments using three-dimensional ceramic/camphene-based co-extrusion. *J. Eur. Ceram. Soc.* **2015**, *35*, 4623–4627. [CrossRef]
82. Yu, M.; Zhou, K.; Zhang, Y.; Zhang, D. Porous Al_2O_3 microspheres prepared by a novel ice-templated spray drying technique. *Ceram. Int.* **2014**, *40*, 1215–1219. [CrossRef]

83. Pawelec, K.M.; Husmann, A.; Best, S.M.; Cameron, R.E. A design protocol for tailoring ice-templated scaffold structure. *J. R. Soc. Interface* **2014**, *11*, 20130958. [CrossRef] [PubMed]
84. Zhang, H. *Ice Templating and Freeze-Drying for Porous Materials and Their Applications*; John Wiley & Sons: Hoboken, NJ, USA, 2018; ISBN 978-3-527-80742-0.
85. De France, K.J.; Hoare, T.; Cranston, E.D. Review of Hydrogels and Aerogels Containing Nanocellulose. *Chem. Mater.* **2017**, *29*, 4609–4631. [CrossRef]
86. Karppinen, A.; Saarinen, T.; Salmela, J.; Laukkanen, A.; Nuopponen, M.; Seppälä, J. Flocculation of microfibrillated cellulose in shear flow. *Cellulose* **2012**, *19*, 1807–1819. [CrossRef]
87. Saarinen, T.; Haavisto, S.; Sorvari, A.; Salmela, J.; Seppälä, J. The effect of wall depletion on the rheology of microfibrillated cellulose water suspensions by optical coherence tomography. *Cellulose* **2014**, *21*, 1261–1275. [CrossRef]
88. Nechyporchuk, O.; Pignon, F.; Belgacem, M.N. Morphological properties of nanofibrillated cellulose produced using wet grinding as an ultimate fibrillation process. *J. Mater. Sci.* **2015**, *50*, 531–541. [CrossRef]
89. Olszewska, A.; Eronen, P.; Johansson, L.-S.; Malho, J.-M.; Ankerfors, M.; Lindström, T.; Ruokolainen, J.; Laine, J.; Österberg, M. The behaviour of cationic NanoFibrillar Cellulose in aqueous media. *Cellulose* **2011**, *18*, 1213. [CrossRef]
90. Fall, A.B.; Lindström, S.B.; Sundman, O.; Ödberg, L.; Wågberg, L. Colloidal Stability of Aqueous Nanofibrillated Cellulose Dispersions. *Langmuir* **2011**, *27*, 11332–11338. [CrossRef] [PubMed]
91. Fukuzumi, H.; Tanaka, R.; Saito, T.; Isogai, A. Dispersion stability and aggregation behavior of TEMPO-oxidized cellulose nanofibrils in water as a function of salt addition. *Cellulose* **2014**, *21*, 1553–1559. [CrossRef]
92. Araki, J. Electrostatic or steric?—Preparations and characterizations of well-dispersed systems containing rod-like nanowhiskers of crystalline polysaccharides. *Soft Matter* **2013**, *9*, 4125–4141. [CrossRef]
93. Peng, Y.; Gardner, D.J.; Han, Y. Drying cellulose nanofibrils: In search of a suitable method. *Cellulose* **2012**, *19*, 91–102. [CrossRef]
94. Velásquez-Cock, J.; Gañán, P.; Gómez, H.C.; Posada, P.; Castro, C.; Dufresne, A.; Zuluaga, R. Improved redispersibility of cellulose nanofibrils in water using maltodextrin as a green, easily removable and non-toxic additive. *Food Hydrocoll.* **2018**, *79*, 30–39. [CrossRef]
95. Dimic-Misic, K.; Maloney, T.; Liu, G.; Gane, P. Micro nanofibrillated cellulose (MNFC) gel dewatering induced at ultralow-shear in presence of added colloidally-unstable particles. *Cellulose* **2017**, *24*, 1463–1481. [CrossRef]
96. Nazari, B.; Kumar, V.; Bousfield, D.W.; Toivakka, M. Rheology of cellulose nanofibers suspensions: Boundary driven flow. *J. Rheol.* **2016**, *60*, 1151–1159. [CrossRef]
97. Nechyporchuk, O.; Belgacem, M.N.; Pignon, F. Current Progress in Rheology of Cellulose Nanofibril Suspensions. *Biomacromolecules* **2016**, *17*, 2311–2320. [CrossRef] [PubMed]
98. Hubbe, M.A.; Tayeb, P.; Joyce, M.; Tyagi, P.; Kehoe, M.; Dimic-Misic, K.; Pal, L. Rheology of Nanocellulose-rich Aqueous Suspensions: A Review. *BioResources* **2017**, *12*, 9556–9661. [CrossRef]
99. Nechyporchuk, O.; Belgacem, M.N.; Pignon, F. Concentration effect of TEMPO-oxidized nanofibrillated cellulose aqueous suspensions on the flow instabilities and small-angle X-ray scattering structural characterization. *Cellulose* **2015**, *22*, 2197–2210. [CrossRef]
100. Martoïa, F.; Dumont, P.J.J.; Orgéas, L.; Belgacem, M.N.; Putaux, J.-L. Micro-mechanics of electrostatically stabilized suspensions of cellulose nanofibrils under steady state shear flow. *Soft Matter* **2016**, *12*, 1721–1735. [CrossRef] [PubMed]
101. Møller, P.C.F.; Rodts, S.; Michels, M.A.J.; Bonn, D. Shear banding and yield stress in soft glassy materials. *Phys. Rev. E* **2008**, *77*, 041507. [CrossRef] [PubMed]
102. Bonn, D.; Denn, M.M.; Berthier, L.; Divoux, T.; Manneville, S. Yield stress materials in soft condensed matter. *Rev. Mod. Phys.* **2017**, *89*, 035005. [CrossRef]
103. Coussot, P. Rheophysics of pastes: A review of microscopic modelling approaches. *Soft Matter* **2007**, *3*, 528–540. [CrossRef]
104. Mohtaschemi, M.; Dimic-Misic, K.; Puisto, A.; Korhonen, M.; Maloney, T.; Paltakari, J.; Alava, M.J. Rheological characterization of fibrillated cellulose suspensions via bucket vane viscometer. *Cellulose* **2014**, *21*, 1305–1312. [CrossRef]

105. Mohtaschemi, M.; Sorvari, A.; Puisto, A.; Nuopponen, M.; Seppälä, J.; Alava, M.J. The vane method and kinetic modeling: Shear rheology of nanofibrillated cellulose suspensions. *Cellulose* **2014**, *21*, 3913–3925. [CrossRef]
106. Derakhshandeh, B.; Petekidis, G.; Shafiei Sabet, S.; Hamad, W.Y.; Hatzikiriakos, S.G. Ageing, yielding, and rheology of nanocrystalline cellulose suspensions. *J. Rheol.* **2012**, *57*, 131–148. [CrossRef]
107. Shafiei-Sabet, S.; Hamad, W.Y.; Hatzikiriakos, S.G. Rheology of Nanocrystalline Cellulose Aqueous Suspensions. *Langmuir* **2012**, *28*, 17124–17133. [CrossRef] [PubMed]
108. Naderi, A.; Lindström, T.; Sundström, J. Carboxymethylated nanofibrillated cellulose: Rheological studies. *Cellulose* **2014**, *21*, 1561–1571. [CrossRef]
109. Siqueira, G.; Kokkinis, D.; Libanori, R.; Hausmann, M.K.; Gladman, A.S.; Neels, A.; Tingaut, P.; Zimmermann, T.; Lewis, J.A.; Studart, A.R. Cellulose Nanocrystal Inks for 3D Printing of Textured Cellular Architectures. *Adv. Funct. Mater.* **2017**, *27*, 1604619. [CrossRef]
110. Dufresne, A. Nanocellulose: A new ageless bionanomaterial. *Mater. Today* **2013**, *16*, 220–227. [CrossRef]
111. Heux, L.; Chauve, G.; Bonini, C. Nonflocculating and Chiral-Nematic Self-ordering of Cellulose Microcrystals Suspensions in Nonpolar Solvents. *Langmuir* **2000**, *16*, 8210–8212. [CrossRef]
112. Lin, N.; Huang, J.; Dufresne, A. Preparation, properties and applications of polysaccharide nanocrystals in advanced functional nanomaterials: A review. *Nanoscale* **2012**, *4*, 3274–3294. [CrossRef] [PubMed]
113. Daud, J.B.; Lee, K.-Y. Surface Modification of Nanocellulose. In *Handbook of Nanocellulose and Cellulose Nanocomposites*; Wiley-Blackwell: Hoboken, NJ, USA, 2017; pp. 101–122, ISBN 978-3-527-68997-2.
114. Missoum, K.; Belgacem, M.; Bras, J.; Missoum, K.; Belgacem, M.N.; Bras, J. Nanofibrillated Cellulose Surface Modification: A Review. *Materials* **2013**, *6*, 1745–1766. [CrossRef] [PubMed]
115. Sofie, S.W.; Dogan, F. Freeze Casting of Aqueous Alumina Slurries with Glycerol. *J. Am. Ceram. Soc.* **2004**, *84*, 1459–1464. [CrossRef]
116. Fukasawa, T.; Ando, M.; Ohji, T.; Kanzaki, S. Synthesis of Porous Ceramics with Complex Pore Structure by Freeze-Dry Processing. *J. Am. Ceram. Soc.* **2001**, *84*, 230–232. [CrossRef]
117. Mariano, M.; da Bernardes, J.S.; Strauss, M. Mold heat conductance as drive force for tuning freeze-casted nanocellulose foams microarchitecture. *Mater. Lett.* **2018**, *225*, 167–170. [CrossRef]
118. Lee, J.; Deng, Y. The morphology and mechanical properties of layer structured cellulose microfibril foams from ice-templating methods. *Soft Matter* **2011**, *7*, 6034–6040. [CrossRef]
119. Jiménez-Saelices, C.; Seantier, B.; Cathala, B.; Grohens, Y. Effect of freeze-drying parameters on the microstructure and thermal insulating properties of nanofibrillated cellulose aerogels. *J. Sol-Gel Sci. Technol.* **2017**, *84*, 475–485. [CrossRef]
120. Munier, P.; Gordeyeva, K.; Bergström, L.; Fall, A.B. Directional Freezing of Nanocellulose Dispersions Aligns the Rod-Like Particles and Produces Low-Density and Robust Particle Networks. *Biomacromolecules* **2016**, *17*, 1875–1881. [CrossRef] [PubMed]
121. Zhai, T.; Zheng, Q.; Cai, Z.; Turng, L.-S.; Xia, H.; Gong, S. Poly(vinyl alcohol)/Cellulose Nanofibril Hybrid Aerogels with an Aligned Microtubular Porous Structure and Their Composites with Polydimethylsiloxane. *ACS Appl. Mater. Interfaces* **2015**, *7*, 7436–7444. [CrossRef] [PubMed]
122. Dash, R.; Li, Y.; Ragauskas, A.J. Cellulose nanowhisker foams by freeze casting. *Carbohydr. Polym.* **2012**, *88*, 789–792. [CrossRef]
123. Svagan, A.J.; Jensen, P.; Dvinskikh, S.V.; Furó, I.; Berglund, L.A. Towards tailored hierarchical structures in cellulose nanocomposite biofoams prepared by freezing/freeze-drying. *J. Mater. Chem.* **2010**, *20*, 6646–6654. [CrossRef]
124. Chen, W.; Yu, H.; Li, Q.; Liu, Y.; Li, J. Ultralight and highly flexible aerogels with long cellulose I nanofibers. *Soft Matter* **2011**, *7*, 10360–10368. [CrossRef]
125. Ali, Z.M.; Gibson, L.J. The structure and mechanics of nanofibrillar cellulose foams. *Soft Matter* **2013**, *9*, 1580–1588. [CrossRef]
126. Kirkwood, D.H. Semisolid metal processing. *Int. Mater. Rev.* **1994**, *39*, 173–189. [CrossRef]
127. Brabazon, D.; Browne, D.J.; Carr, A.J. Mechanical stir casting of aluminium alloys from the mushy state: Process, microstructure and mechanical properties. *Mater. Sci. Eng. A* **2002**, *326*, 370–381. [CrossRef]
128. Cai, H.; Sharma, S.; Liu, W.; Mu, W.; Liu, W.; Zhang, X.; Deng, Y. Aerogel Microspheres from Natural Cellulose Nanofibrils and Their Application as Cell Culture Scaffold. *Biomacromolecules* **2014**, *15*, 2540–2547. [CrossRef] [PubMed]

129. Ishwarya, S.P.; Anandharamakrishnan, C.; Stapley, A.G.F. Spray Freeze Drying. In *Handbook of Drying for Dairy Products*; Wiley-Blackwell: Hoboken, NJ, USA, 2017; pp. 123–148, ISBN 978-1-118-93052-6.
130. Wang, Q.; Sun, J.; Yao, Q.; Ji, C.; Liu, J.; Zhu, Q. 3D printing with cellulose materials. *Cellulose* **2018**, *25*, 4275–4301. [CrossRef]
131. Håkansson, K.M.; Henriksson, I.C.; de la Peña Vázquez, C.; Kuzmenko, V.; Markstedt, K.; Enoksson, P.; Gatenholm, P. Solidification of 3D Printed Nanofibril Hydrogels into Functional 3D Cellulose Structures. *Adv. Mater. Technol.* **2016**, *1*, 1600096. [CrossRef]
132. Li, V.C.-F.; Dunn, C.K.; Zhang, Z.; Deng, Y.; Qi, H.J. Direct Ink Write (DIW) 3D Printed Cellulose Nanocrystal Aerogel Structures. *Sci. Rep.* **2017**, *7*, 8018. [CrossRef] [PubMed]
133. Nissilä, T.; Karhula, S.S.; Saarakkala, S.; Oksman, K. Cellulose nanofiber aerogels impregnated with bio-based epoxy using vacuum infusion: Structure, orientation and mechanical properties. *Compos. Sci. Technol.* **2018**, *155*, 64–71. [CrossRef]
134. Wang, M.; Shao, C.; Zhou, S.; Yang, J.; Xu, F. Preparation of carbon aerogels from TEMPO-oxidized cellulose nanofibers for organic solvents absorption. *RSC Adv.* **2017**, *7*, 38220–38230. [CrossRef]
135. Yang, H.; Yan, R.; Chen, H.; Lee, D.H.; Zheng, C. Characteristics of hemicellulose, cellulose and lignin pyrolysis. *Fuel* **2007**, *86*, 1781–1788. [CrossRef]
136. Donius, A.E.; Liu, A.; Berglund, L.A.; Wegst, U.G.K. Superior mechanical performance of highly porous, anisotropic nanocellulose–montmorillonite aerogels prepared by freeze casting. *J. Mech. Behav. Biomed. Mater.* **2014**, *37*, 88–99. [CrossRef] [PubMed]
137. Köhnke, T.; Elder, T.; Theliander, H.; Ragauskas, A.J. Ice templated and cross-linked xylan/nanocrystalline cellulose hydrogels. *Carbohydr. Polym.* **2014**, *100*, 24–30. [CrossRef] [PubMed]
138. Li, W.L.; Lu, K.; Walz, J.Y. Freeze casting of porous materials: Review of critical factors in microstructure evolution. *Int. Mater. Rev.* **2012**, *57*, 37–60. [CrossRef]
139. Sehaqui, H.; Zhou, Q.; Ikkala, O.; Berglund, L.A. Strong and Tough Cellulose Nanopaper with High Specific Surface Area and Porosity. *Biomacromolecules* **2011**, *12*, 3638–3644. [CrossRef] [PubMed]
140. Nemoto, J.; Saito, T.; Isogai, A. Simple Freeze-Drying Procedure for Producing Nanocellulose Aerogel-Containing, High-Performance Air Filters. *ACS Appl. Mater. Interfaces* **2015**, *7*, 19809–19815. [CrossRef] [PubMed]
141. Kasraian, K.; DeLuca, P.P. Thermal Analysis of the Tertiary Butyl Alcohol-Water System and Its Implications on Freeze-Drying. *Pharm. Res.* **1995**, *12*, 484–490. [CrossRef] [PubMed]
142. Tang, Y.; Qiu, S.; Wu, C.; Miao, Q.; Zhao, K. Freeze cast fabrication of porous ceramics using tert-butyl alcohol–water crystals as template. *J. Eur. Ceram. Soc.* **2016**, *36*, 1513–1518. [CrossRef]
143. Lu, Z.; Su, Z.; Song, S.; Zhao, Y.; Ma, S.; Zhang, M. Toward high-performance fibrillated cellulose-based air filter via constructing spider-web-like structure with the aid of TBA during freeze-drying process. *Cellulose* **2018**, *25*, 619–629. [CrossRef]
144. Fall, A.B.; Lindström, S.B.; Sprakel, J.; Wågberg, L. A physical cross-linking process of cellulose nanofibril gels with shear-controlled fibril orientation. *Soft Matter* **2013**, *9*, 1852–1863. [CrossRef]
145. Naderi, A.; Lindström, T. Carboxymethylated nanofibrillated cellulose: Effect of monovalent electrolytes on the rheological properties. *Cellulose* **2014**, *21*, 3507–3514. [CrossRef]
146. Sehaqui, H.; Zhou, Q.; Berglund, L.A. High-porosity aerogels of high specific surface area prepared from nanofibrillated cellulose (NFC). *Compos. Sci. Technol.* **2011**, *71*, 1593–1599. [CrossRef]
147. Svagan, A.J.; Samir, M.A.S.A.; Berglund, L.A. Biomimetic Foams of High Mechanical Performance Based on Nanostructured Cell Walls Reinforced by Native Cellulose Nanofibrils. *Adv. Mater.* **2008**, *20*, 1263–1269. [CrossRef]
148. Chau, M.; De France, K.J.; Kopera, B.; Machado, V.R.; Rosenfeldt, S.; Reyes, L.; Chan, K.J.W.; Förster, S.; Cranston, E.D.; Hoare, T.; et al. Composite Hydrogels with Tunable Anisotropic Morphologies and Mechanical Properties. *Chem. Mater.* **2016**, *28*, 3406–3415. [CrossRef]
149. Smeets, N.M.B.; Bakaic, E.; Patenaude, M.; Hoare, T. Injectable poly(oligoethylene glycol methacrylate)-based hydrogels with tunable phase transition behaviours: Physicochemical and biological responses. *Acta Biomater.* **2014**, *10*, 4143–4155. [CrossRef] [PubMed]
150. Toll, S. Note: On the tube model for fiber suspensions. *J. Rheol.* **1993**, *37*, 123–125. [CrossRef]

151. Orgéas, L.; Dumont, P.J.J.; Vassal, J.-P.; Guiraud, O.; Michaud, V.; Favier, D. In-plane conduction of polymer composite plates reinforced with architectured networks of Copper fibres. *J. Mater. Sci.* **2012**, *47*, 2932–2942. [CrossRef]
152. Martoïa, F.; Dumont, P.J.J.; Orgéas, L.; Belgacem, M.N.; Putaux, J.-L. On the origins of the elasticity of cellulose nanofiber nanocomposites and nanopapers: A micromechanical approach. *RSC Adv.* **2016**, *6*, 47258–47271. [CrossRef]
153. Woignier, T.; Reynes, J.; Hafidi Alaoui, A.; Beurroies, I.; Phalippou, J. Different kinds of structure in aerogels: Relationships with the mechanical properties. *J. Non-Cryst. Solids* **1998**, *241*, 45–52. [CrossRef]
154. Ma, H.-S.; Roberts, A.P.; Prévost, J.-H.; Jullien, R.; Scherer, G.W. Mechanical structure–property relationship of aerogels. *J. Non-Cryst. Solids* **2000**, *277*, 127–141. [CrossRef]
155. Yang, X.; Cranston, E.D. Chemically Cross-Linked Cellulose Nanocrystal Aerogels with Shape Recovery and Superabsorbent Properties. *Chem. Mater.* **2014**, *26*, 6016–6025. [CrossRef]
156. Wang, M.; Anoshkin, I.V.; Nasibulin, A.G.; Korhonen, J.T.; Seitsonen, J.; Pere, J.; Kauppinen, E.I.; Ras, R.H.A.; Ikkala, O. Modifying Native Nanocellulose Aerogels with Carbon Nanotubes for Mechanoresponsive Conductivity and Pressure Sensing. *Adv. Mater.* **2013**, *25*, 2428–2432. [CrossRef] [PubMed]
157. Wang, M.; Anoshkin, I.V.; Nasibulin, A.G.; Ras, R.H.; Laine, J.; Kauppinen, E.I.; Ikkala, O. Electrical behaviour of native cellulose nanofibril/carbon nanotube hybrid aerogels under cyclic compression. *RSC Adv.* **2016**, *6*, 89051–89056. [CrossRef] [PubMed]
158. Zheng, Q.; Cai, Z.; Ma, Z.; Gong, S. Cellulose Nanofibril/Reduced Graphene Oxide/Carbon Nanotube Hybrid Aerogels for Highly Flexible and All-Solid-State Supercapacitors. *ACS Appl. Mater. Interfaces* **2015**, *7*, 3263–3271. [CrossRef] [PubMed]
159. Zhou, S.; Wang, M.; Chen, X.; Xu, F. Facile Template Synthesis of Microfibrillated Cellulose/Polypyrrole/Silver Nanoparticles Hybrid Aerogels with Electrical Conductive and Pressure Responsive Properties. *ACS Sustain. Chem. Eng.* **2015**, *3*, 3346–3354. [CrossRef]
160. Deville, S.; Maire, E.; Bernard-Granger, G.; Lasalle, A.; Bogner, A.; Gauthier, C.; Leloup, J.; Guizard, C. Metastable and unstable cellular solidification of colloidal suspensions. *Nat. Mater.* **2009**, *8*, 966–972. [CrossRef] [PubMed]
161. Deville, S.; Adrien, J.; Maire, E.; Scheel, M.; Di Michiel, M. Time-lapse, three-dimensional in situ imaging of ice crystal growth in a colloidal silica suspension. *Acta Mater.* **2013**, *61*, 2077–2086. [CrossRef]
162. Albouy, P.A.; Deville, S.; Fulkar, A.; Hakouk, K.; Impéror-Clerc, M.; Klotz, M.; Liu, Q.; Marcellini, M.; Perez, J. Freezing-induced self-assembly of amphiphilic molecules. *Soft Matter* **2017**, *13*, 1759–1763. [CrossRef] [PubMed]